論文 / 著書情報
Article / Book Information

題目(和文)	
Title(English)	A study on the application of digital holography in digital pathology
著者(和文)	SyukranHakim
Author(English)	Hakim Syukran
出典(和文)	学位:博士(工学), 学位授与機関:東京工業大学, 報告番号:甲第11587号, 授与年月日:2020年9月25日, 学位の種別:課程博士, 審査員:山口 雅浩,中本 高道,金子 寛彦,小尾 高史,渡辺 義浩
Citation(English)	Degree:Doctor (Engineering), Conferring organization: Tokyo Institute of Technology, Report number:甲第11587号, Conferred date:2020/9/25, Degree Type:Course doctor, Examiner:,,,,
学位種別(和文)	博士論文
Type(English)	Doctoral Thesis

TOKYO INSTITUTE OF TECHNOLOGY

Interdisciplinary Graduate School of Science and Engineering

4259, Nagatsuta, Midori-ku, Yokohama 226-8503, Japan

Doctoral Thesis

A study on the application of digital holography in digital pathology

Supervisor:
Professor Masahiro Yamaguchi

Tokyo Institute of Technology
Interdisciplinary Graduate School of Science and Engineering
Department of Information Processing

Syukran Hakim Bin Norazman

Table of contents

Abstract

In recent years, along with the development of computational power and image processing, a new field called digital pathology has been developed to aid pathologist in diagnosing disease. In this field, the tissue (histological) or cell (cytological) samples taken are from patients are digitally imaged through slide scanning system instead of observed through microscope. Then, features such as morphological structure, tissue pattern are extracted from the images using image processing algorithm. Using these data, an automated classification system can be developed to identify the severity of the disease. This technique is beneficial to create a fast and accurate diagnosis pipeline, helping the pathologist and ensuring better life expectancy for patients.

Nevertheless, there are still many challenges and problems that need to be tackled in digital pathology. For example, current imaging system and algorithm developed for digital pathology centralize around color image. Thus, the samples still need to go through standard staining procedure which can be time consuming. Fortunately, there are several studies that have been done to integrate quantitative phase imaging such as digital holography into digital pathology. This method does not require staining procedure as the imaging principle is based material's refractive index instead of absorption. Despite this efforts, current works only focus on integrated phase while textural features that are widely used in color image are not yet fully explored in phase image. Moreover, because most studies in phase imaging centered on live transparent cells and not stained tissue or cells, the relationship between phase and color information in histological sample is not well known. Another challenge is when imaging thick samples, scanner that has low depth of field will require multiple acquisition in Z-axis. Digital holography could offer image refocusing from a single digital hologram, but it only works for coherent image.

In this study, a hybrid optical system that combines incoherent (bright-field) and coherent (digital holography) imaging was developed. This system is used to capture the color image and digital hologram of stained cytological sample (malignant lymphocytes) and the phase distribution was analyzed. The color image is used to assist segmentation process of the overlapping cells. From the experimental analysis, the spatially-averaged phase mean value of malignant lymphocytes has larger dispersion compared to normal cells. This information can be exploited for malignant lymphoma identification in digital pathology. The study also confirmed that the cell phase value is correlated with its size, regardless the cells are stained and enclosed in mounting media.

Next, an analysis of quantitative phase of Hematoxylin and Eosin stained histological sample was conducted. Here, using previously mentioned hybrid imaging system, the phase and color image of liver tissue were captured. After that, the relationship between phase and color textural information inside nuclear region was investigated. From the analysis, this study discovered that texture features obtained from phase image could provide different information from the color image. The most apparent distinction between normal and cancer nuclei in phase image was observed in the Grey-Level Co-occurrence Matrix contrast and homogeneity. This unique feature is beneficial for classifying the liver tissue into Hepatocellular Carcinoma (HCC) or normal cases. Another advantage in using phase image in classification is the possibility of using unstained samples, thus faster pathological diagnosis can be conducted.

Finally, by taking the advantage of the hybrid coherent and incoherent imaging system, a novel image processing technique was developed. This method enables 3-D reconstruction and refocusing of color object from bright-field image by using information from digital holography as support. The algorithm exploits the sparsity of the 3D objects and reconstruct it from digital hologram using compressive holography. Next, a binary mask is created to separate the object from transparent voxels. The binary mask is then used to assist 3-D color object reconstruction from a bright-field image. After that, image refocusing can be conducted by applying convolution operator between the reconstructed

object and the 3-D point spread function. The effectiveness of this algorithm was demonstrated in a simulation of simple object and cytological cells phantoms. In these simulations, the reconstructed objects achieved good match with ground truth. This method has potential to be applied for 3-D pathological imaging without requiring the acquisition of z-stack images.

As for conclusion, this study explored the application of quantitative phase image via digital holography for both cytological and histological samples by developing a hybrid coherent and incoherent imaging system. For cyto-pathological field, this study contributed in the identification of malignant lymphocytes from phase distribution of stained sample. For histo-pathological field, this study explored the unique textural feature in phase image and its application in classifying HCC cases and the possibility of using unstained sample in diagnosis. Lastly, this study developed a novel 3-D reconstruction algorithm for application in imaging thick samples in digital pathology.

Abstract (Japanese)

本論文は "A study on the application of digital holography in digital pathology（デジタルホログラフィーのデジタル病理診断への応用に関する研究）" と題し、英文 6 章から構成されている。

第 1 章 "Introduction（序論）" では、本研究の背景として、デジタル病理学と呼ばれる新しい分野の発展と課題について論じている。具体的には、従来の病理診断は、患者から採取した組織や細胞サンプルの顕微鏡観察を基本とするものであるのに対して、デジタル病理診断は、スライドスキャナを用いて得られる超高精細デジタル画像に基づくワークフローの革新により、迅速かつ正確な診断へ貢献するとともに、画像解析技術を応用した診断支援などの発展をもたらしていると述べている。一方で、生体組織は透明であるため、一般的な病理診断では染色の工程を経て視覚化する必要があるが、デジタルホログラフィー（DH）のような定量的な位相イメージング技術を応用することで、染色工程を経ずに組織を視覚化する技術も研究されていることを紹介している。しかし、従来の DH による位相イメージングで得られる像は、染色病理標本で観察される特徴との関係が明らかになっていない点が課題として挙げられている。これらの議論に基づき、本研究の目的は、DH をデジタル病理学に融合することで、病理診断の高度化に貢献する技術を具現化することであるとしている。

第 2 章 "Background（背景）"では、本論文に関連する技術分野として、デジタル病理学、DH、位相計測に基づく細胞のイメージング、明視野顕微鏡と DH の組み合わせなどに関して従来研究を概観し、本研究の新規性を明らかにしている。

第 3 章 "Quantitative phase imaging for stained cytological sample（染色細胞診標本の定量位相イメージング）" では、本研究で開発したインコヒーレント（明視野）イメージングとコヒーレント（DH）イメージングを組み合わせたハイブリッドシステムを紹介し、その細胞診標本への応用に関して実験結果を示している。このシステムでは、カラー画像は、重なり合っている細胞のセグメンテーション処理に利用され、細胞ごとの位相変調量取得を可能にしている。このシステムを用いて、染色された悪性リンパ腫の細胞診標本のカラー画像とデジタルホログラムを撮影し、位相分布を解析した結果、悪性リンパ腫の位相平均値は正常細胞と比較して大きく分散していることを示している。これらの結果から、提案した明視野画像解析と位相計測を組み合わせる解析手法は、悪性細胞の同定などに活用できると述べている。

第 4 章 "Quantitative phase analysis on H&E stained histopathological sample（H&E 染色病理組織標本の定量位相解析）" では、従来の一般的な病理組織染色手法であるヘマトキシリンとエオシンで染色した組織標本の定量的な位相の解析を行っている。ここでは、先述のハイブリッドイメージングシステムを用いて、肝臓組織標本の位相とカラー画像を撮影し、核領域内の位相と色のテクスチャ情報の関係を調べている。その結果、位相画像から得られるテクスチャ特徴はカラー画像とは異なる情報を提供する可能性があることを見出した。特に、位相画像における濃度共起行列のコントラストと均質性の特徴において、肝細胞癌と正常組織に分類するのに有益であったことを示している。そして、本手法を用いれば無染色の標本を使用して診断できるため、より迅速な病理診断が可能になる

可能性があると述べている。

第 5 章 "Three-dimensional image processing for application in digital pathology（デジタル病理学応用に向けた３次元画像処理）" では、本研究で開発したハイブリッドイメージングシステムの利点を生かす新しい３次元画像処理手法を提案し

ている。提案する手法では、DH の情報をサポートとして用いることで、明視野画像からのカラー物体の 3 次元再構成とリフォーカスを可能にしている。３次元再構成のアルゴリズムは３次元物体の空間的なスパース性を利用しており、圧縮ホログラフィーの概念を用いて DH から再構成した画像により３次元ボクセル中にバイナリマスクを作成し、このバイナリマスクをサポートとして明視野画像からの３次元カラー物体の再構成を行っている。その後、再構成された物体と３次元点像分布関数の畳み込みによりリフォーカス処理を可能としている。そして、単純な物体と細胞ファントムを用いた計算機シミュレーションにより本アルゴリズムの有効性が示されている。この手法は、光軸方向の焦点走査を必要としないため、高速な３次元病理イメージングに応用できる可能性を有していると述べている。

第 6 章 "Conclusion （結論）" では、本論文で得られた成果を総括している。以上を要するに、本論文では、コヒーレントとインコヒーレントのハイブリッドなイメージングシステムを開発し、染色病理標本と定量的な位相画像情報の融合が細胞病理学及び病理組織学分野のイメージング技術の発展をもたらす可能性を示したものであり、工学上ならびに工業上において寄与するところが大きい。よって、本論文は博士（工学）の学位論文として価値あるものと認められる。

Chapter 1

Introduction

1.1 Research Introduction

Over the span of human history, we had witnessed and went through countless of diseases and epidemic. Our survival instincts had led us to investigate the cause and signs of those disease in order to find cure and thus elude mortality. This knowledge is also known as pathology, derived from ancient Greek word *pathos* (suffering) and *-logy* (study of). Pathology includes the specific examination and dissecting of body parts.

Perhaps the biggest leap in understanding disease or more generally the biological structure of living things can be traced back to the invention of microscope. Through the glass lenses we learned how the cells work, discovering the DNA, the mechanism of bacteria and viruses or any other pathogen that can cause disease.

In conventional modern pathology, the study can be divided into two main groups which are cytology, the study of cells and histology, the study of tissues. In either case, the diagnosis process starts with pathologist taking samples from patient. Samples that are resected via surgery or biopsy is called histological sample while samples that are in form of cell clusters suspended in liquid is known as cytological sample. The approach depends on organs and what type of disease is being diagnosed.

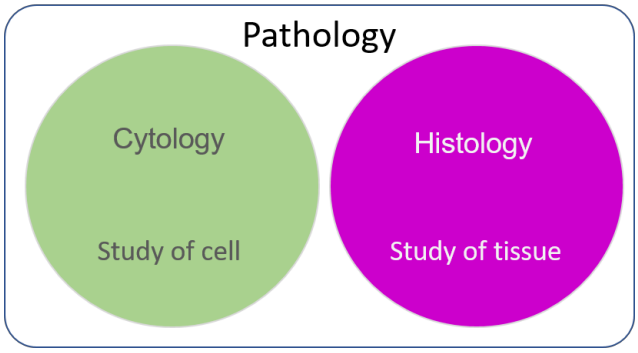

Fig 1.1: Branch of study in pathological field

Biological tissues are mostly colorless and transparent. So, in the next step the samples are stained to increase the contrast. Furthermore, different dye components will color different parts of the tissue sample, thus helping the pathologist to get better understanding of the tissue structure. Typically, Hematoxylin and Eosin (HE) are used as staining dye for histological sample. By using this stain, the nuclei region will be colored in blue-purple while cytoplasm will become pink-red, as shown in figure below.

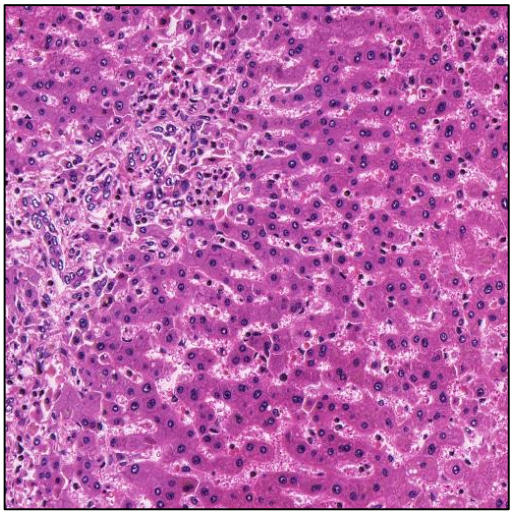

Fig 1.2: Liver tissue stained with H&E

The choosing of staining dye depends on tissue and cell types, diseases and what particular information that the pathologist wish to get. Other stains examples are Papanicolaou stain (commonly used for cytological sample) and Ki67 immunochemistry stain (used as indicator for cancer).

For example, figure below shows the malignant mesothelioma cells that are stained with Papanicolaou stain. This dye will give cytoplasm green color while the nuclei will be colored in blue.

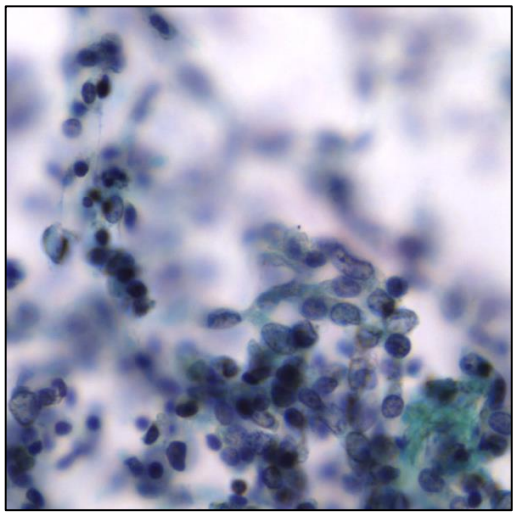

Fig 1.3: Malignant mesothelioma cells stained with Papanicolaou

In more advance technique, fluorescence markers are used to detect certain type of proteins inside the cells. It is worth noted that staining procedure require high amount of expertise to be properly done. Lack of experience can cause the samples to be damaged or under/over-stained and hindering the diagnosis process. Depending on stain types, this procedure can also be time consuming.

In the final step, the sample are placed onto glass slide and observed through a microscope. To ensure the longevity of the sample, it is fixed using a clear mounting media. Generally, a bright-field microscopy is to view the samples, but in some cases fluorescence microscopy and phase contrast microscopy are also utilized.

In case of phase imaging, the technique utilizes the light phase difference caused by the object to create grayscale image, instead of light absorption in case of bright-field imaging. This is useful for imaging live cells and does not require the staining process. In more advance technique, the exact phase difference can be measured using quantitative phase imaging such as digital holography. The example of phase image of liver tissue captured using digital holography is shown in next figure.

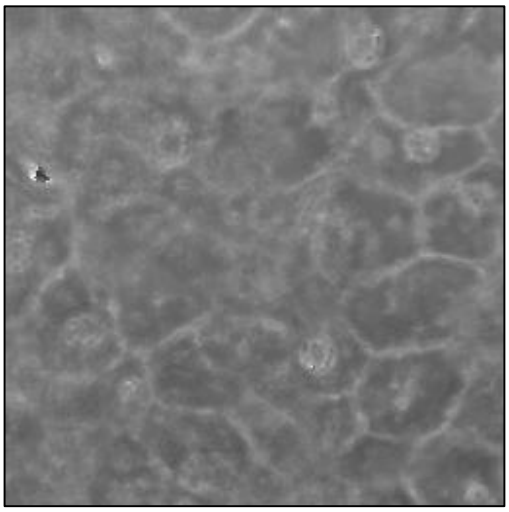

Fig 1.4: Phase image of liver tissue captured using digital holography

After the imaging process is completed, the pathologist will analyze the disease from the captured image and determine which grade and stage does it belongs to (in case of cancer) and provide the prognosis.

Recently, pathology is coming to a new age where computer power and image processing technique are being used to further empower the field. The pathological samples can now be digitally scanned and processed using computers. This technique, also known as digital pathology will help pathologist to quickly and accurately diagnose the disease. [1-5]

One of the most useful tools that empower digital pathology is the Whole Slide Image (WSI) scanner. By using this scanner, pathologist can quickly scan the sample slide into digital images. WSI scanner is usually equipped with high precision motorized stage, thus sample can be scanned and properly stitched into large image to help pathologist get better overview during diagnosis.

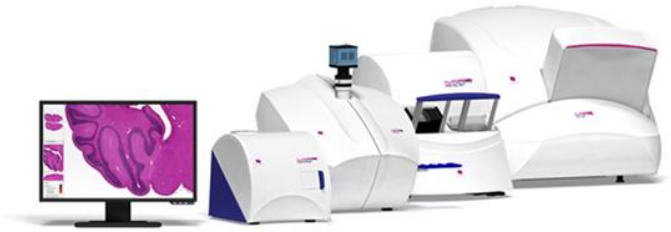

Fig 1.5: Whole Slide Image scanner (Copyright 3D Histech)

Moreover, with the rise of computational power and the decrease of computing cost, cutting edge image processing technique can be applied to scanned sample images. Conventional diagnosis flow can be rewritten as computer algorithm. The tissue structures such as nuclear size, density, texture etc. can now be calculated using image processing technique and quantitatively analyzed. This gives the birth of computer-assisted diagnosis which not only can help the pathologist diagnosis the disease faster but more accurate.

Nevertheless, current technique in digital pathology mainly revolves around color imaging. Thus, the samples still need to be prepared through staining procedures which could be time consuming.

Several approaches have been proposed to bring phase imaging into digital pathology e.g. by developing automatic slide scanner that utilize quantitative phase imaging (Fig 1.6). However, these approaches are mainly focused on diagnosis based on integrated phase or density of the sample. The relationship between phase (refractive index) distribution and morphology visualized by staining is not yet well clarified

Fig 1.6: Commercial Digital Holographic Microscope (Copyright Lynceetec)

1.2 Challenges and open problems in digital pathology

Digital pathology has a great potential to revolutionize the medical field. However, there are certain challenges that need to be overcame before it can be adopted by mainstream.

First, most slide scanners developed for digital pathology are based on bright-field microscopy. Thus, most diagnosis algorithm are tailored to use color image. Nevertheless, quantitative phase imaging is slowly being adopted into the digital pathology especially for imaging live cytological samples. The phase image could give additional information to further increase the diagnosis accuracy.

However, current analysis for phase image is mainly based on measuring the integrated phase of cytological samples. Little to none study has been conducted on application of quantitative phase measurement for stained cytological and histological samples.

Application of texture features, which are commonly used in color image of histological samples, need to be investigated for phase image as well. Moreover, due the fact that phase imaging is commonly used for unstained samples, the relationship between stain and phase distribution is not yet known. The combinations are summarized in table below.

Imaging system	Staining	Sample	Analysis
Bright-field	Stained	Cytology	Morphology, texture
Quantitative phase	Unstained	Cytology	Morphology, Integrated phase
Bright-field	Stained	Histology	Morphology, texture
Quantitative phase	Stained	Cytology	Integrated phase
Quantitative phase	Stained	Histology	Texture

Table 1.1: Combinations of imaging system, samples and analysis method for digital pathology. Green rows are commonly developed techniques. Yellow rows are yet to be explored.

Another problem arises when imaging thick samples using a slide scanner that has low depth of field (due to trade-off of high numerical aperture). Here, a large set of Z-stack images need to be acquired to capture the whole 3D structure of the sample. It would be beneficial to develop a system that can quickly capture the 3D object without multiple scanning in Z-axis.

1.3 Objective of study

The first goal of this study is to find the relationship between stain and phase distribution inside pathological image. In order to achieve this, an optical system that can capture both color and phase image need to be constructed. In this study, a bright-field imaging and digital holographic microscope will be used to achieve the objective.

The next objective is to calculate and analyze textural features extracted from both color and phase image. The textural features inside phase image has not been clearly investigated. It would be important to examine whether these features are similar to texture features extracted from color image. This information will be useful to develop pathological diagnosis without staining procedure.

Finally, a novel image processing technique that combine coherent (digital holography) and incoherent (bright-field) imaging will be develop. This is to achieve image refocusing which is not possible in incoherent imaging. The developed algorithm can be later utilized for imaging pathological sample without the need of z-stack acquisition.

1.4 Thesis structure

This thesis is divided into 6 chapters. In first chapter, the introduction of this study will be explained. In second chapter, the background and research works related to this study will be briefly reviewed. In chapter 3, a hybrid optical system that combine bright-field and digital holography will be proposed and applied to image stained cytological sample. In chapter 4, the same optical system is used to analyze phase texture features of stained histopathological sample. In chapter 5, a novel image processing technique that allows 3D reconstruction of color object from bright-field image and digital hologram will be proposed. Finally, in chapter 6 the summary and conclusion for each chapter will be stated.

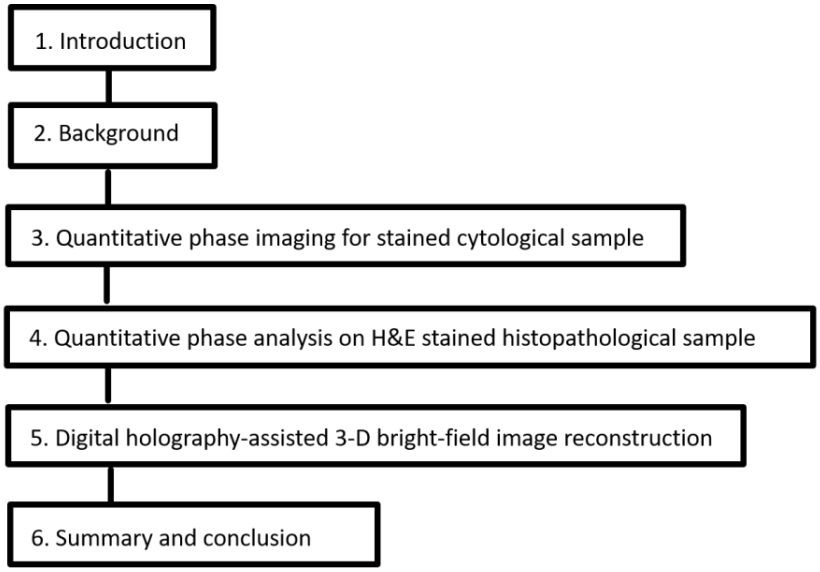

Fig 1.7: Thesis structure

The main research themes in this thesis will be divided into 3 chapters i.e. chapter 3 to chapter 5. The connection between these chapters is visualized in figure below. In nutshell, chapter 3 covers the application of quantitative phase measurement of stained cytological cell while chapter 4 covers the stained histological tissue. In chapter 5, 3D imaging component from digital holography is incorporated for the application in general digital pathology.

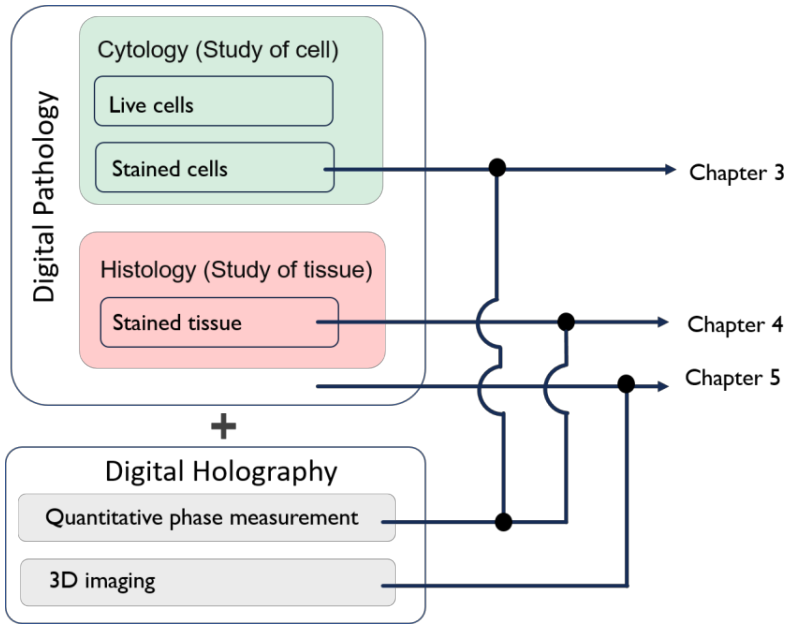

Fig 1.8: Connection between chapters (3-5)

Chapter 2

Background

In this chapter, a more detailed reviews on development of digital pathology, digital holography and related research involving phase measurement of cells will be elaborated. Then, the intuition and standpoint of this study will be explained.

2.1 Related works

2.1.1 On digital pathology

Since the end of 1960's, pathologist started to develop telepathology where pathological images were transferred across different parts of the worlds. This enables pathological diagnosis, education and research at a distance. As the communication and computers advances, these technologies were soon adapted into pathological field. For example, pathological slide can now be imaged using a device called whole slide scanner (WSS). WSS can offer full automatic imaging at higher speed compared to conventional microscope.

Currently, digital pathology not only signify the diagnosis of disease, but is an umbrella terms that covers the whole field of pathology such as sample imaging, data management, image processing, disease classification etc.

2.1.2 On digital holography

Holography was first developed by Dennis Gabor in 1946 using electron beam and earned him a Nobel Prize. However, the practical use of holography using light was only possible starting 1960's after the invention of laser. Later, the invention of optoelectronic devices such as CCD and CMOS enables the hologram to be recorded digitally instead of on a photographic film, which gives the birth of digital holography. Soon after, the

application of digital holography in acquiring images of microscopic objects were widely developed.

The utilization of digital holography for stained pathological sample was first proposed by (X. Mo et. al. 2009) They developed RGB digital holographic microscopy to capture the amplitude and quantitative phase distribution of stained intestine tissue. The study is a mainly a proof of concept and revolved around the ability of digital holography in refocusing tissue image. No further analysis on the phase distribution was conducted.

2.1.3. On cell's refractive index and phase measurement

(P. Wang et. al 2010) conducted a research on statistical refractive index properties of cell internal structure. They stated that refractive index distribution have a great potential for cancer diagnosis and screening which is undetectable using conventional cytopathology. They proposed a practical approach to measure the distribution using Statistical Amplitude Microscopy (SAM) and demonstrated its application for detecting intestinal cancer.

(R. K. Bista et. al 2011) conducted a study to find a link between nuclear refractive index and cell cycle. They found that nuclear refractive index is highly correlated with the increase of DNA content. They argued that the increase of nuclear refractive index in malignant and normal cells from cancer patients is caused by abnormal DNA replication and mitosis. Nuclear refractive index was suggested as a new indicator for early cancer detection.

(Hoa V. Pham et. al 2016) proposed a diagnosis method for urothelial carcinoma using quantitative phase imaging (QPI). They measured and analyzed the quantitative phase of unstained cells from urine cytology. The total nuclear mass was estimated and utilized as an indicator to classify the disease malignancy.

(Xiaoxu Lu et.al 2012) proposed a technique to reconstruct 3D profile of biological sample using digital holographic microscopy. The research mainly focused on correcting

the phase aberration caused by the objective lens. The aberration was eliminated using image correlation algorithm and digital phase mask.

2.1.4. On nuclear structure and its relation to cancer

It is well accepted that cancer growth is related to cell cycle, particularly the irregular DNA replication in the cell nuclei. Thus, studying the structure inside cell nuclear is important during pathological analysis.

(F. N. Ghadially 1997) mentioned that the nucleoli morphology can be categorized into two types, open and compactly structured. However, the importance of these variations is not clear. Generally, open nucleolus signifies an active cell while compact nucleolus is the opposite. Interestingly, in tumors both types together with intermediate structure can be seen.

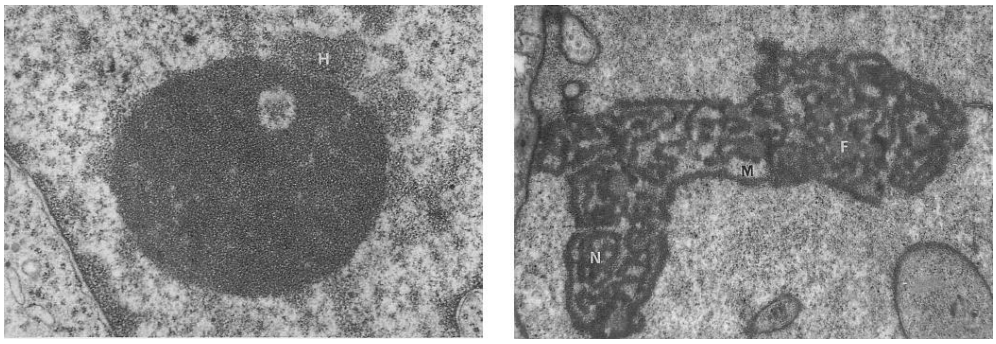

Fig 2.1: Image of nucleoli from transmission electron microscope (Copyright F. N. Ghadially 1997). Left: Compactly structured. Right: Openly structured

In more recent study, (Cherkezyan et al. 2014) discovered that chromatin distribution inside cell nuclei can be utilized for early carcinogenesis. Figure below shows the apparent difference in chromatin structure between nuclei from normal rectal and colorectal cancer cells.

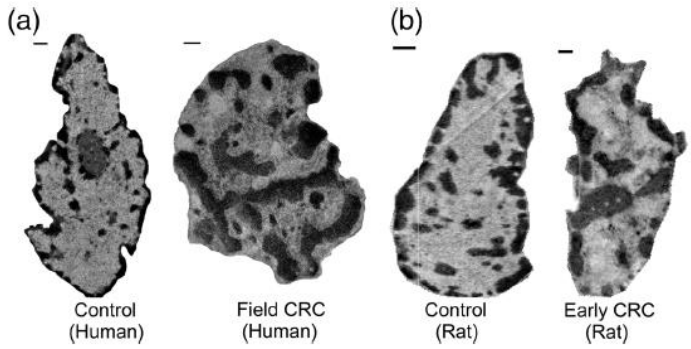

Fig 2.2: a) Normal nuclei from control patients and a pre-cancerous adenoma representing field CRC. Scale bars: 500 nm. b) Normal colonic cell nuclei from control rats and early CRC. Scale bars: 250 nm. (Copyright Cherkezyan et al. 2014)

On related topic, (F. Kimura 2018) explored the possibility of determining Ki-67 expressions by analyzing hematoxylin-and-eosin-stained (HE) stained nuclei images from endometrial adenocarcinoma of the uterine corpus. Despite their high success rate in separating the nuclei, the main challenge is the signal intensity because the nuclei region is stained with same dye component i.e. Hematoxylin.

2.1.5. On hybrid bright-field (BF) and digital holographic (DH) imaging system

During the inception of this research, not many research that combines BF and DH imaging system were available in the literature. This is because BF system is mainly used to image color (amplitude) objects while DH's strongest advantage is imaging transparent (phase) objects. Nevertheless, one interesting example is a study by (N. Pavillon et.al. 2012).

In their study, they used a hybrid BF and DH system to detect cell death. The BF was used to capture color image of sample stained with trypan blue, while DH measured the quantitative phase. By analyzing the correlation between these two information, they concluded that quantitative phase from DH can be utilized for early and label-free detection of cell death.

In a more recent report, (Byeon et.al 2016) conducted a study on cell dynamics using hybrid BF and DH system. In their work, the distinct T-cell adhesion dynamics on inflamed endothelial layers was successfully captured. The hybrid system was used to take the advantage of 3D refocusing in DH and high contrast imaging in BF.

2.1 Research intuition and standpoint

As summarized in previous section, digital pathological field is widely being developed. There are several research works are being conducted to bring quantitative phase imaging into digital pathology. Yet, these works are mainly focused on live, unstained cytological samples. Furthermore, the analysis is focused on integrated phase. It would be interesting to study the phase texture of nuclei inside stained sample, particularly the histological samples.

In addition, it is important to clarify what this thesis does not cover in scope of digital pathology and digital pathology. First, this study focuses on imaging (stained cells and tissues) and feature analysis in digital pathology. Thus, other topics such as molecular pathology, monitor-based diagnosis, digital data management etc. will not be discussed. From digital holography point of view, this study will mainly utilize the quantitative phase measurement and 3D imaging. Other application such as digital holographic data storage and compression, cryptography, display, optical tweezer will not be part of this thesis. It is also worth mentioning that despite chapter 6 involves 3D color object reconstruction multispectral digital holography will not be covered.

Chapter 3

Quantitative phase imaging for stained cytological sample

In this chapter, the principle behind optical system used in this research will be explained. In order to capture both digital hologram and color bright-field image, a hybrid optical system was developed.

3.1 Principle of digital hologram

Light can be modeled as a wave with complex amplitude. The complete recording of wave information i.e. amplitude and phase is called hologram. In comparison to incoherent imaging such as bright-field imaging, the captured information is actually interference pattern between object's wave and reference wave.

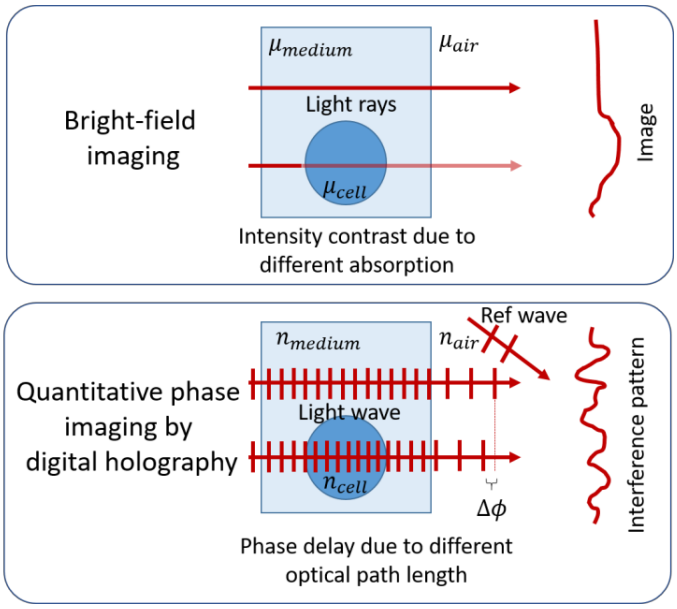

Fig 3.1: Comparison between bright-field imaging and digital holography

In order to capture a hologram, first consider a coherent point light source which its spatial phase difference is constant. This light source is collimated to create a plane wave.

The plane wave is split into two, creating object and reference waves, which are coherent to each other.

The object wave is now used to illuminate a semi-transparent object and the light wave coming out from the object can be expressed as:

$$\mathrm{u}(x,y) = |u(x,y)| \exp[j\phi(x,y)] \quad (3.1)$$

The object wave then propagates until it reaches to a plane where the imaging device is placed. There are multiple models that can be used to calculate this propagation, depending on the distance, object size and sampling criteria. Since this study mainly revolves around near-field imaging, Fresnel approximation can be used. Alternatively, angular spectrum (AS) method can also be used.

The object wave interferes with the reference wave,

$$\mathrm{r}(x,y) = |r(x,y)| \exp[j\psi(x,y)] \quad (3.2)$$

which is directed at a slight off-angle, creating an interference pattern, i.e. the hologram.

The interference pattern can be expressed as:

$$\mathrm{a}(x,y) = |u(x,y) + r(x,y)|^2 = |\mathrm{u}(x,y)|^2 + |\mathrm{r}(x,y)|^2 + 2|\mathrm{u}(x,y)||\mathrm{r}(x,y)| \cos[\psi(x,y) - \phi(x,y)] \quad (3.3)$$

In practice, an objective lens is placed between object and imaging device to create an enlarged image. However, this will introduce a curved phase into the captured wave. If the exact curve is known, the aberration can be eliminated by multiplying the object wave digitally with a conjugated phase. Multiple techniques exist to precisely estimate and compensate the curvature, either through physical optical system or digital filter In this study, the phase curvature is estimated by capturing hologram when no object is placed in front of the objective. The final phase image is compensated digitally based on the estimated curvature.

To extract the object wave from the hologram, a FFT-method can be used. (Takeda 1998). By calculating the Fourier transform of the hologram, the carrier and object spectrum are separated in Fourier domain. Then by simply shifting the object spectrum to origin, and calculating the inverse Fourier transform, the object wave can be recovered.

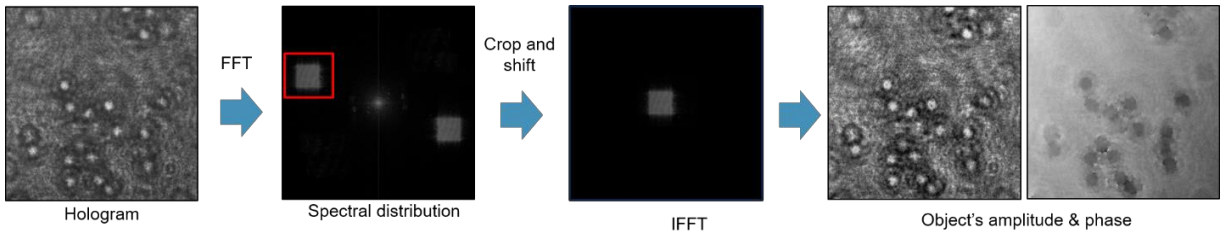

Fig 3.2: Extracting object's complex amplitude wave from digital hologram

This technique also known as off-axis holography. The complex amplitude of the object wave can calculated using a single captured hologram at the cost of spatial resolution. However, by optimizing the image magnification and the off-axis angle, a diffraction limited imaging system can be achieved.

3.2 Optical system: Hybrid color and phase imaging

The optical system used in this study is composed of a combination of a Mach–Zehnder interferometer and a bright-field microscopy, which enables us to capture both hologram and RGB image of a sample.

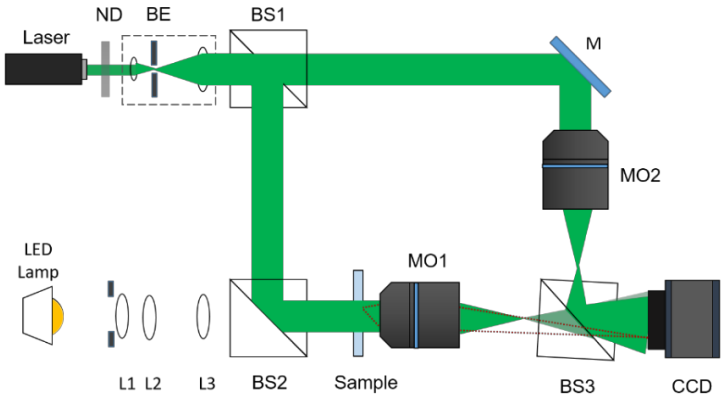

Fig 3.3: Optical setup

In a holographic mode of the system, the sample is illuminated with a diode pumped green laser, while a white LED is used for a bright-field mode. The sample image is magnified using an objective lens. The hologram and color image of the sample are recorded by a charge-coupled device (CCD) camera. The symbol and description are listed below.

Symbol	Description	Specification
ND	Natural Density filter	
BE	Beam expander	Aperture 50um
MO1,MO2	Objective lens	40x NA 0.75
M	Mirror	
L1,L2,L3	Lens	
BS1,BS2	Beam splitter	
CCD	CCD camera	Flovel FD-420 Pixel size: 6.7 micron Resolution: 1300x1024
Laser	Laser	Green laser 532 nm

Table 3.1: Symbol description of optical system

The laser wavelength need to be carefully considered when imaging a stained samples using a single wavelength laser. For example, in case of Papanicolaou dye which makes the sample green and blue, green laser is acceptable. For Hematoxylin and Eosin stained samples, the absorption peak for Hematoxylin and Eosin are 590nm and 530 nm respectively. Thus, a blue or red laser is more suitable as it can penetrate both parts. If the object wave SNR too low, the interference pattern contrast will be lower thus object wave cannot be precisely recovered.

Conventional microscope utilizes Kohler illumination to create a uniform illumination and at the same time preventing the image of light source to be appear on imaging plane. This optical system use 3 lenses to achieve similar result. The first lens act

as collector and collimate the LED light. The second lens act as a field lens, focusing the collector's light onto condenser lens, creating a narrower collimated beam.

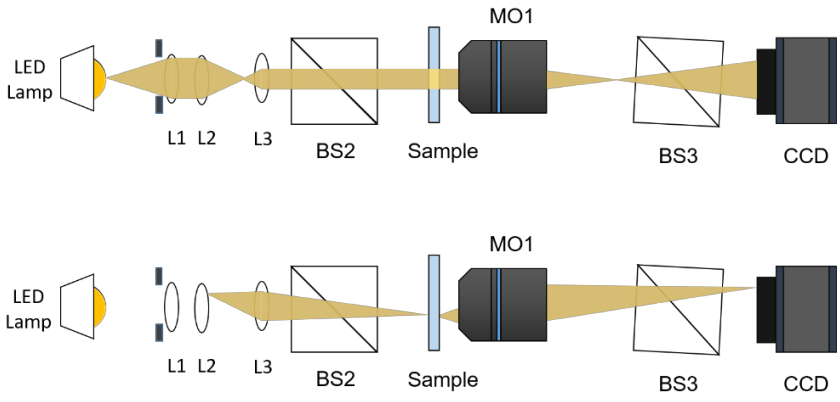

Fig 3.4: Illumination in bright-field mode

Here, a frosted LED body is used to reduce its coherency which can create fringe artifact in the final color image. In contrast to conventional microscope that uses halogen lamp, this setup does not utilize blue filter as most of color correction and white balance processing can be done digitally. Another advantage is LED produce less heat as contrast to halogen lamp than can cause air turbulence to the surrounding of optical system and affecting the phase measurement.

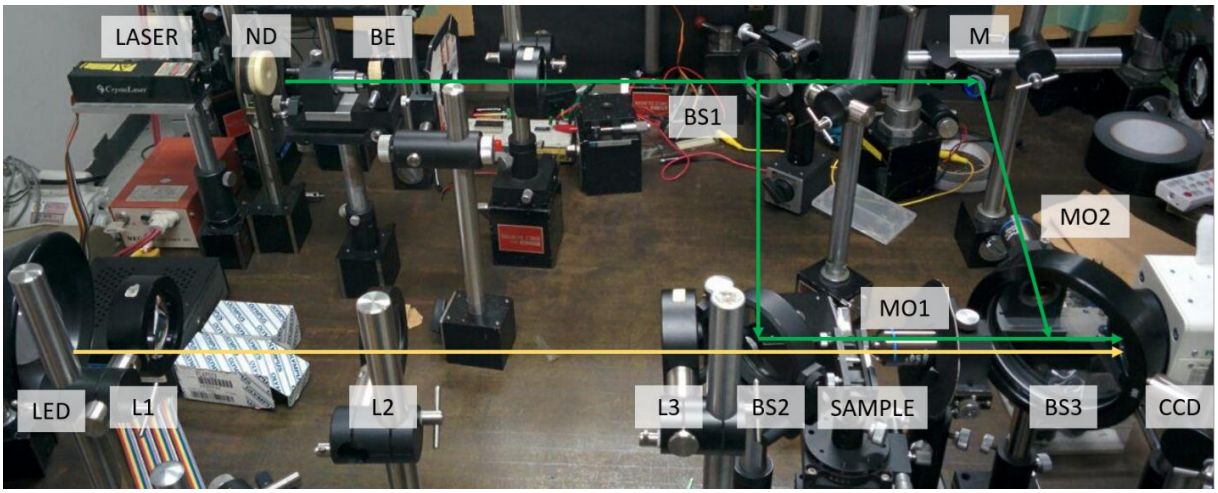

Fig 3.5: Optical system

Figure above is the real implementation of the optical system. The green line shows the light path of laser beam for digital holography acquisition. The yellow line shows the light path of the LED lamp for the bright-field image acquisition.

3.3 Color and phase imaging of cytological samples

In this section, the hybrid color and digital holographic system will be used to image cytological sample. A brief background will be described and experiment procedures, result and discussion will follow.

3.3.1 Background

The death caused by malignant lymphoma, a type of cancer has been increasing every year. One of the methods to diagnose malignant lymphoma is aspiration cytology (R.K. Gupta et. Al 2003). However, differentiation between malignant lymphoma from reactive lesion in cytological examination can be difficult and has been a long standing issue to be solved.

In this study, a hybrid color digital holographic microscope was used to capture the phase image of lymphocytes (refer figure below) to discover any possible feature which can be used for improving malignant lymphoma cells identification.

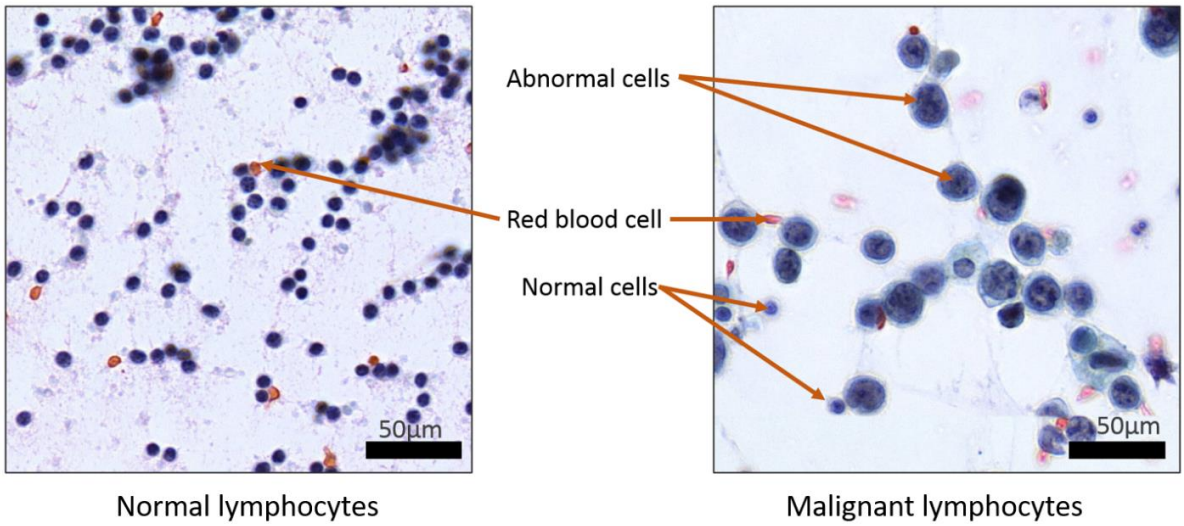

Fig 3.6: Normal and malignant lymphocytes imaged with Whole Slide Image (WSI) scanner

3.3.2 Experiment flow

First, the Fresnel hologram and RGB image of normal and malignant lymphocytes were captured using the hybrid imaging system. Then, the object wave information was extracted from the hologram using the fast Fourier transform (FFT) calculation. Next, the Fresnel back-propagation was applied to bring the hologram image into focus. Consequently, the phase image was calculated from hologram image. Afterwards, the locations and regions of individual cells were determined using watersheds segmentation algorithm.

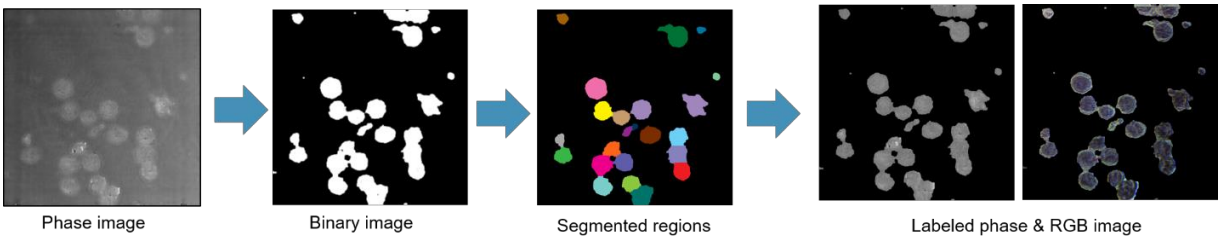

Fig 3.7: Watershed algorithm for cell segmentation

Finally, the spatially averaged phase value for each cell is calculated by taking the division of a total phase value over the total cell area.

3.3.3 Results and discussion

The figure shows the color image where background was removed and phase image with pseudo color of lymphocytes. The left side shows the results of malignant lymphocytes, and the right side indicates the normal cells. The malignant lymphocytes have not only larger size but also higher phase values compared to normal lymphocytes.

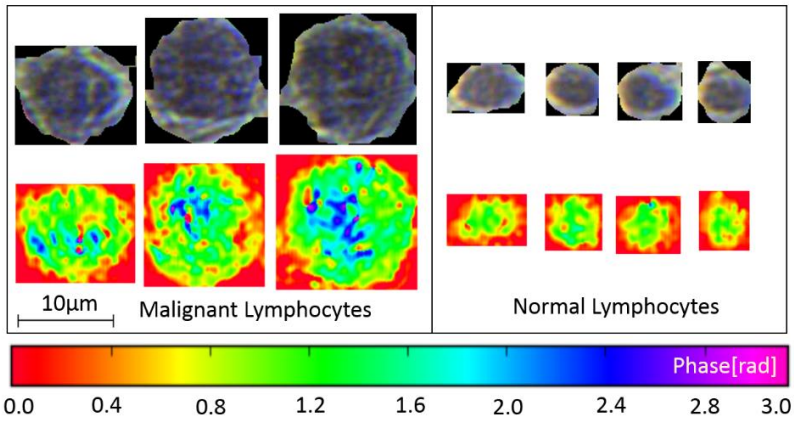

Fig 3.8: Color and phase image of malignant and normal cells

However, since phase value is related to object thickness, it might be better to normalize the phase value by cell size. The histogram of spatially averaged phase values for malignant and normal cases is shown in figure below.

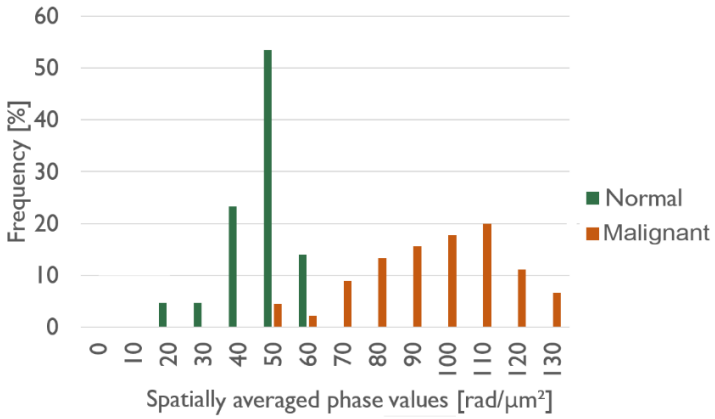

Fig 3.9: Histogram of spatially averaged phase values

It appears that the mean of the spatially averaged phase of malignant cells is larger than in the normal ones. This can explained by the fact that the malignant cells are bigger, thus thicker than the normal cells. The large variance shown in the malignant case is interesting because it might suggest that the inner phase, i.e. refractive-index distribution of malignant cells is different compared to normal cells. This feature has a potential to be further utilized for malignant lymphoma identification.

3.3.4. Conclusion

The color image and phase distributions of normal and malignant lymphocytes was captured using a hybrid imaging system. By experimental investigation, the spatially-averaged mean value of malignant lymphocytes has larger dispersion compared to normal cells which can be exploited for malignant lymphoma identification purpose. It is worth noted that in cytological case, the phase values is highly related to its size. Thus in future it might be better to use samples that has similar size in order to get better understanding on the inner phase distribution. Finally, the color image in this section was not directly used the statistical analysis, but serves as reference for diagnosis.

Chapter 4

Quantitative phase analysis on H&E stained histopathological sample

This chapter focuses on the analysis of quantitative phase of HE stained sample. First, a brief background and motivation of this study are introduced. Then, the experiment workflow and image processing procedures are explained. Next, the result and discussion are reported.

4.1. Histopathological images in digital pathology

Recently, digital pathology have been actively developed to supports cancer diagnosis using computerized image analysis and machine learning of digitized histopathological image. Stained tissue samples are (e.g. H&E staining) are imaged using digital microscopy and the tissue structure are analyzed to diagnose the disease.

Usually important morphological features such as the nuclear structure, i.e. the nuclear size, shape and chromatin texture inside the nuclei are observed. Several methods have been proposed to quantify and characterized the nuclear textures for cancer diagnosis.

4.2. Phase measurement of histopathological images

Application of phase measurement such as phase contrast and digital holography (DH) into cell imaging is also widely utilized, especially for living (transparent) cells. These methods are useful because the sample doesn't need to be stained. Here, DH is more advantageous compared to phase contrast microscopy as it can give contrast in form of quantitative phase. This information is physically related to optical thickness i.e. refractive index of the samples. Moreover, quantitative phase is more suitable for standardization and computer-based diagnosis. Not only that, as its name implies, DH is consist of whole light wavefront information, so 3D image refocusing is feasible.

Several research works have been conducted to apply DH for cell and tissue imaging. However, these studies mainly revolves on the integrated phase information that is linked to the size or thickness of cells. A more detail investigation on phase texture features are yet to be conducted.

The crucial question here is: Does the phase image obtained from DH gives same texture information as in color image? Let say the texture features in phase image and color image are correlated to each other, then we can assume that conventional image analysis techniques for digital or pathology in general, can be used on the phase image of unstained sample. However, if they are not related to each other, i.e., phase textures provides new texture information relative to color texture, then we can use both features to further improvise the diagnosis accuracy in stained sample. Either way, both outcomes are beneficial from digital pathology point of view.

4.3. Objective of study

The objective of this study is to analyze the relationship between both information by comparing the textural features taken from bright-field and phase images. Next, application of the calculated features for classification of Hepatocellular Carcinoma (HCC), a type of liver cancer is investigated.

4.4. Experiment workflow

4.4.1. Optical system

An optical system that combines an off-axis digital holographic and a bright-field microscopy similar to the one mentioned in previous chapter was used to image the pathological samples. One major difference is the laser wavelength used for DH illumination, which was changed to red 632nm. This is to allow the object beam to penetrate both nuclei and cytoplasm region considering Hematoxylin and Eosin spectral absorption is highest at approximately 590nm and 530nm respectively.

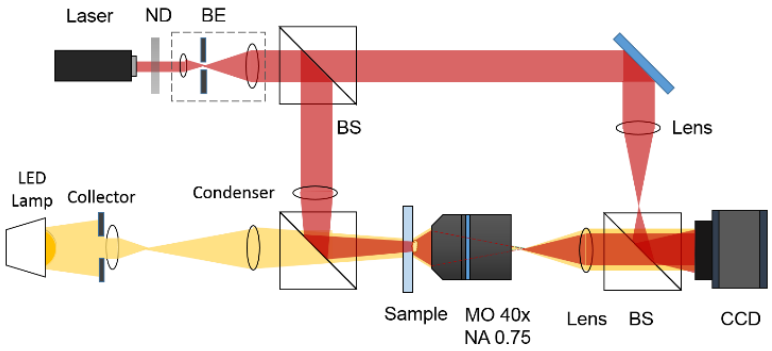

Fig 4.1: Optical setup

4.4.2. Histopathological sample

Hepatocellular Carcinoma (HCC) positive liver tissue (grade 1-3 Edmondson and Steiner Grading System) and the adjacent normal liver tissues were used in this study. Every tissue core has 5µm thickness and stained using H&E staining. These cores were embedded in a tissue micro array glass slide (Biomax LV723).

For each case (Normal, Grade 1, Grade2, Grade 3: N,G1,G2,G3) , three cores (a,b,c) were selected. This gave 12 tissue samples in total. The summary of N, G1, G2, G3 cases are listed in Table 4.1. The image of tissue cores are shown in Fig. 4.2 and 4.3.

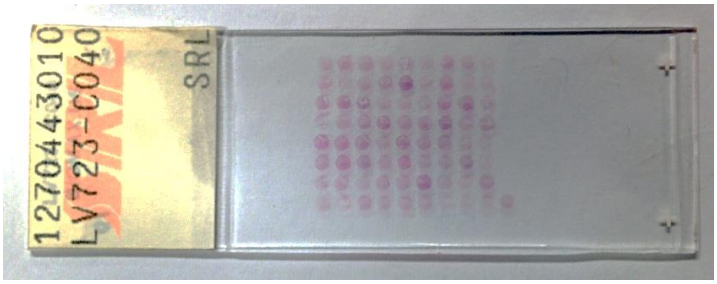

Fig 4.2: Tissue micro array

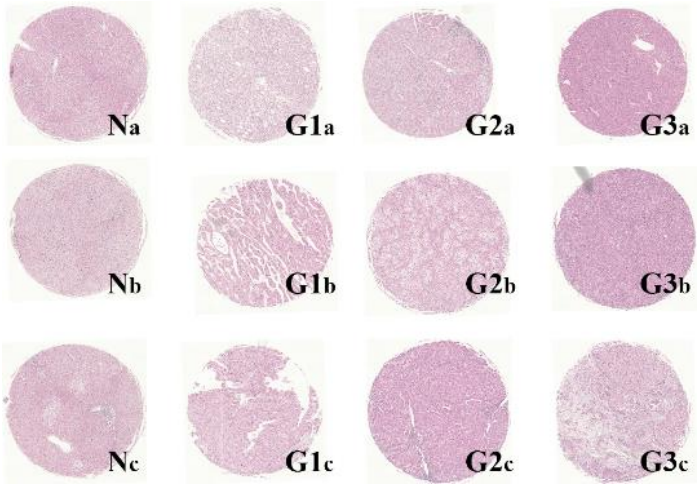

Fig 4.3: Tissue cores

Sample	Sex	Age	Pathology Diagnosis
Na	M	60	Cancer adjacent normal tissue
Nb	M	34	Cancer adjacent normal tissue
Nc	M	31	Cancer adjacent normal tissue
G1a	M	50	HCC grade 1
G1b	M	71	HCC grade 1
G1c	M	56	HCC grade 1
G2a	M	38	HCC grade 2
G2b	M	35	HCC grade 2
G2c	M	40	HCC grade 2
G3a	M	63	HCC grade 3
G3b	M	47	HCC grade 3
G3c	F	48	HCC grade 3

Table 4.1: Details on each liver tissue sample

4.4.3. Experiment procedures

The experiment was conducted as follows. First, the tissue slide was placed onto imaging stage and the bright-field (RGB) image and digital hologram of the samples were captured. The hologram was captured as an image-hologram, where it was in the same plane as color image. Multiple region of interest (ROI) were captured by moving the stage in XY-axis.

Next, image processing procedures were applied. For color image, a simple white balance processing was done to correct the RGB ratio and the image was converted to grayscale by taking the average of the 3 channels. For hologram, the object wave was reconstructed using fast Fourier Transform (FFT) algorithm. The phase image was calculated by taking the argument of the complex-valued object wave. Phase compensation was done by estimating the aberration curve from a non-object hologram that was captured beforehand. Since the distance from hologram plane to image plane is zero, no wave propagation calculation was needed. In the next step, a phase unwrapping algorithm was applied to the phase image. Consequently, the phase image was converted to grayscale by linearly mapping 0~10.5 radian to 0~255.

4.4.4. Nuclei segmentation

This study focuses on nuclei textural features, thus an image processing technique to extract nuclei region from the pathological samples was employed. An algorithm proposed by (Wienert S. et. al. 2012) was used as base and slightly modified to suit this research requirement. The nuclei process consists of 6 major steps, where the 4^{th} step was an original modification.

4.4.4a. Detection of all closed contours

The grayscale image was used as input image. First, a contour seed was selected where the intensity gradient is maximum. Then, the contour was traced as long as the intensity resides between a local minimum and local maximum value. That contour was considered valid if it returns to the original location, with the same angle as starting step.

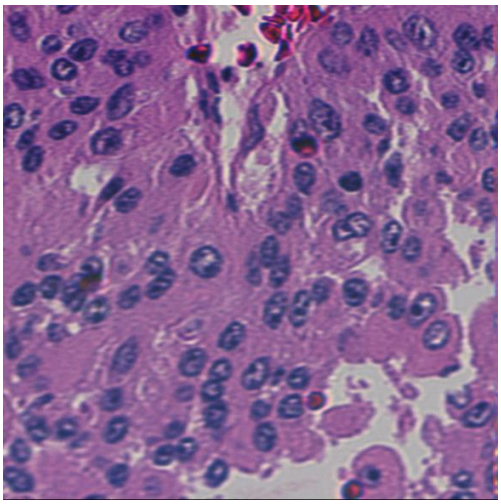

Fig 4.4: Input color image

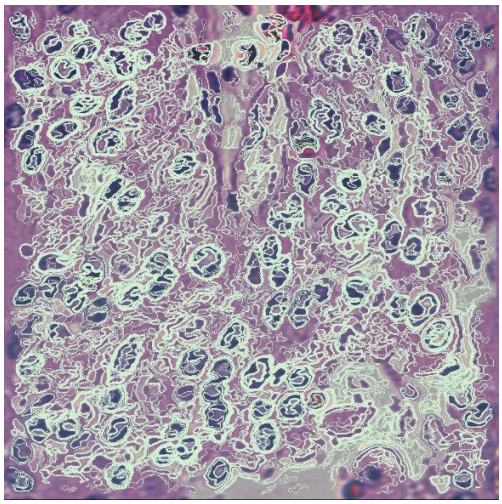

Fig 4.5: Detected contours drawn on color image

4.4.4b. Contour evaluations

Next, each contour was evaluated, i.e. given a score depending on how well it separates object and background. The score was calculated using method defined as follows:

I. Apply a Sobel filter to input image → imgS
II. For each contour on imgS, calculate the mean pixel value covered by the contour.

4.4.4c. Generation of non-overlapped contours

In this step, the contours were sorted based on their score. Then, each contour was drawn onto image if it did not overlap with other contour, prioritizing contour with highest score first.

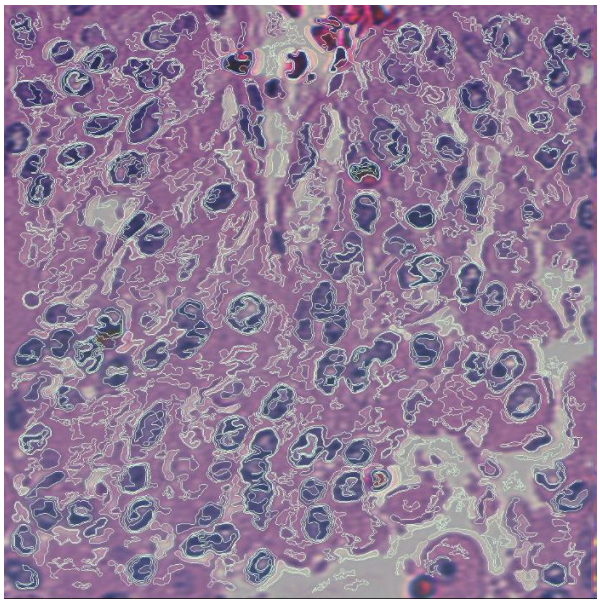

Fig: 4.6: Non-overlapping contours

4.4.4d. Contour grouping

A problem arose when applying conventional method to cancer positive images. In those cases, the nuclei envelopes were disconnected those resulting poor segmentation and contour appearing in another contour.

To overcome this, contours that were enclosed with a bigger contour were grouped together. Contours with no child nor parent were removed. Then an active contour model, SNAKE was used to smoothen the detected parent contours. Then the best contour from the group was selected based on its circularity.

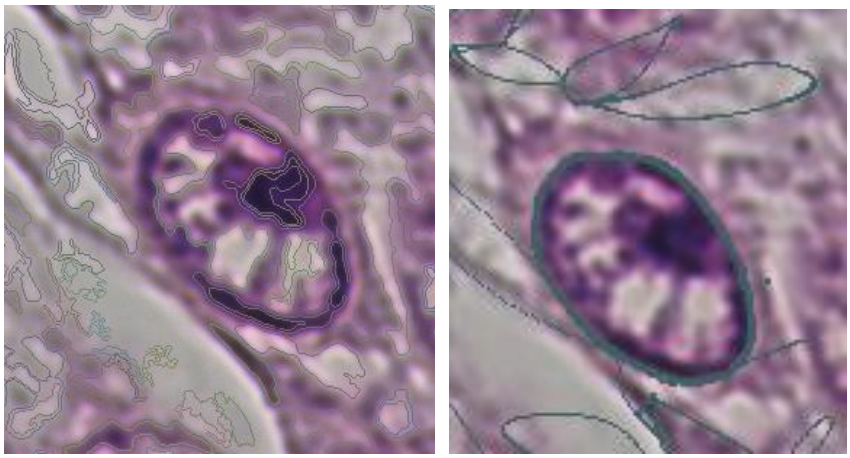

Fig: 4.7: Segmentation result after algorithm modification

4.4.4e. Concave splitting

In this step, clustered nuclei were split into individual nucleus. Some splitting errors might occurs.

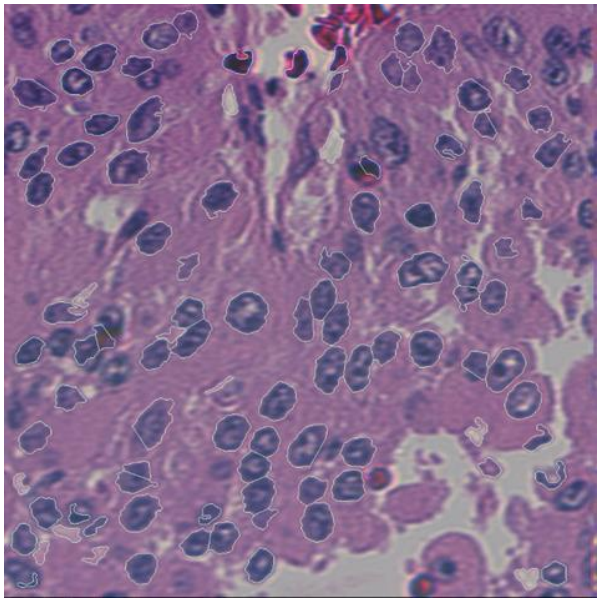

Fig 4.8 : Contour after concave splitting

4.4.4f. Nuclei and non-nuclei classification

In this final step, the contours were classified into nuclei or non-nuclei object based on its staining properties. A color deconvolution process was applied to the RGB image to separate the H&E components.

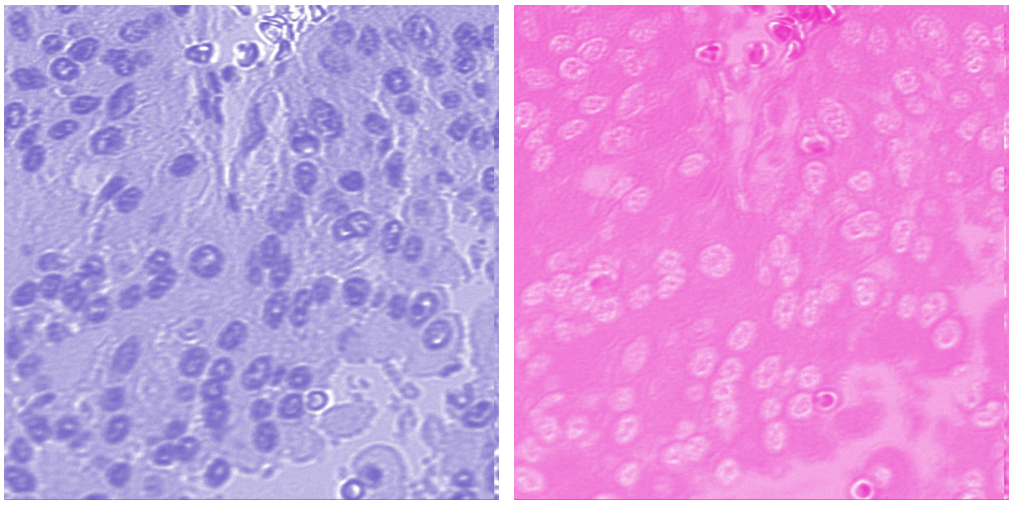

Fig 4.9: H&E component from color deconvolution

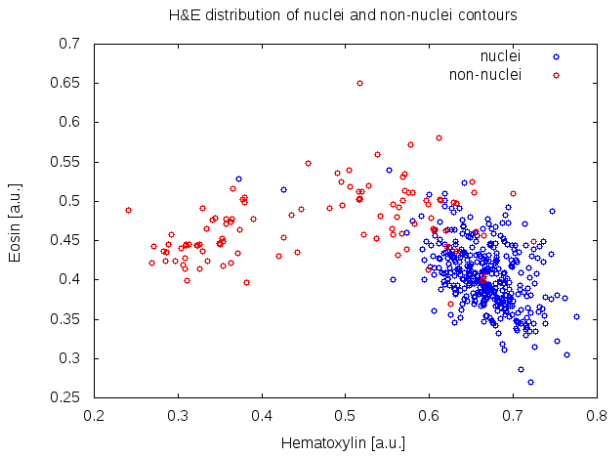

Fig. 4.10: H&E distribution of nuclei and non-nuclei

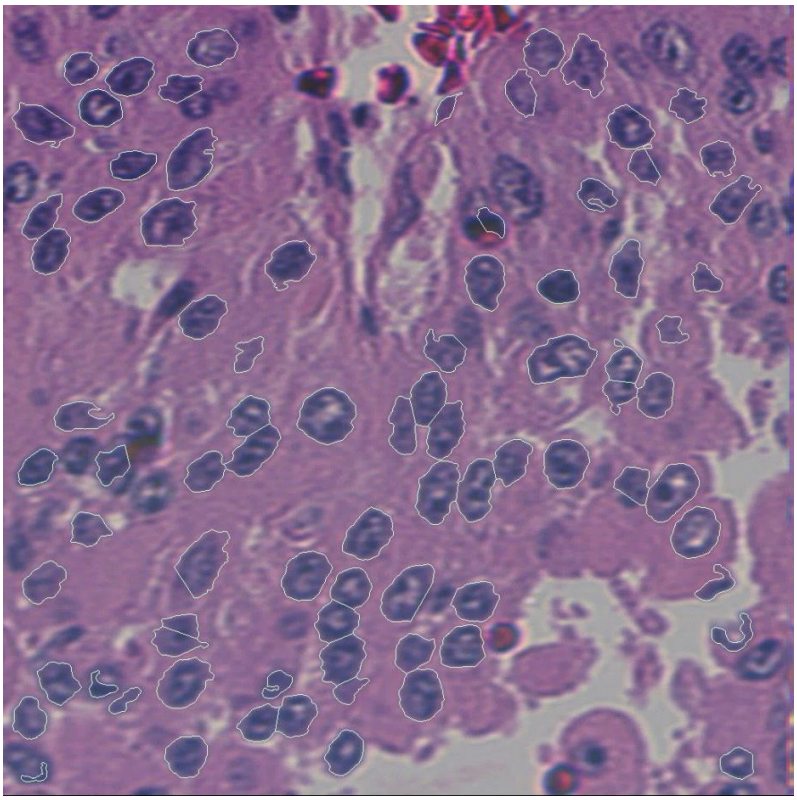

Fig 4.11: Final segmentation result

The resulting nuclei contour was utilized later as mask during the texture and morphological feature calculation.

4.4.5. Texture and morphological features calculation

In this study, both morphological and textural features were measured. For morphological features, nuclei area and perimeter were calculated from the resulting segmented nuclei region explain previously.

For texture analysis, Grey Level Co-occurrence Matrix features were used on grayscale phase and bright-field images. Additionally, the mean and standard deviation of phase inside each nucleus are also computed. Nearly 100 arbitrary nuclei were selected from each sample and used for this calculation.

The GLCM algorithm is explained as follows. Using grayscale image as input, every pixel bounded by nuclei contour was evaluated. The values between each pixel and its neighboring pixels were tallied into a co-occurrence matrix.

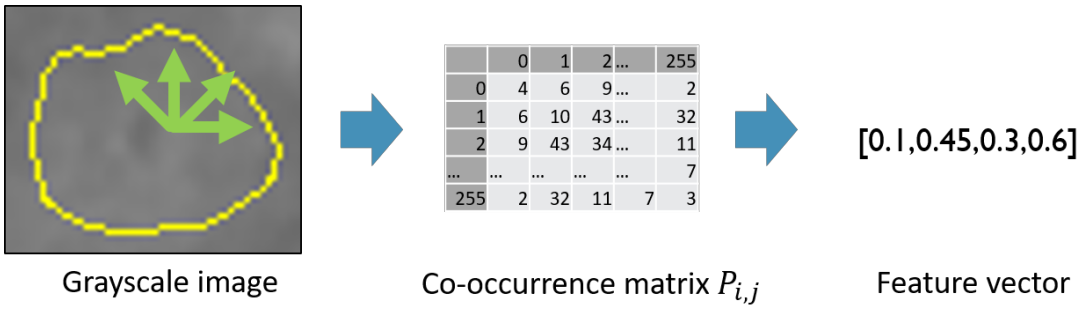

Fig 4.12: GLCM algorithm

Three commonly used features in HCC classification (Angular Second Moment (ASM), homogeneity, contrast) were calculated for every nuclei in each sample. The GLCM features were computed using 2 pixels offset in 4 directions (0, 45, 90, 135°) and the maximum value was used. The definition for each feature is written below.

GLCM Contrast: $\sum_{i,j=0}^{levels-1} P_{i,j}(i-j)^2$

GLCM Homogeneity: $\sum_{i,j=0}^{levels-1} P_{i,j} \frac{1}{1+(i-j)^2}$

GLCM Angular Second Moment (ASM): $\sum_{i,j=0}^{levels-1} P_{i,j}^2$

4.5. Results and discussions

Figures below shows the examples of bright-field (left) and phase image (right) of the samples. The yellow line indicates the segmented nuclei region.

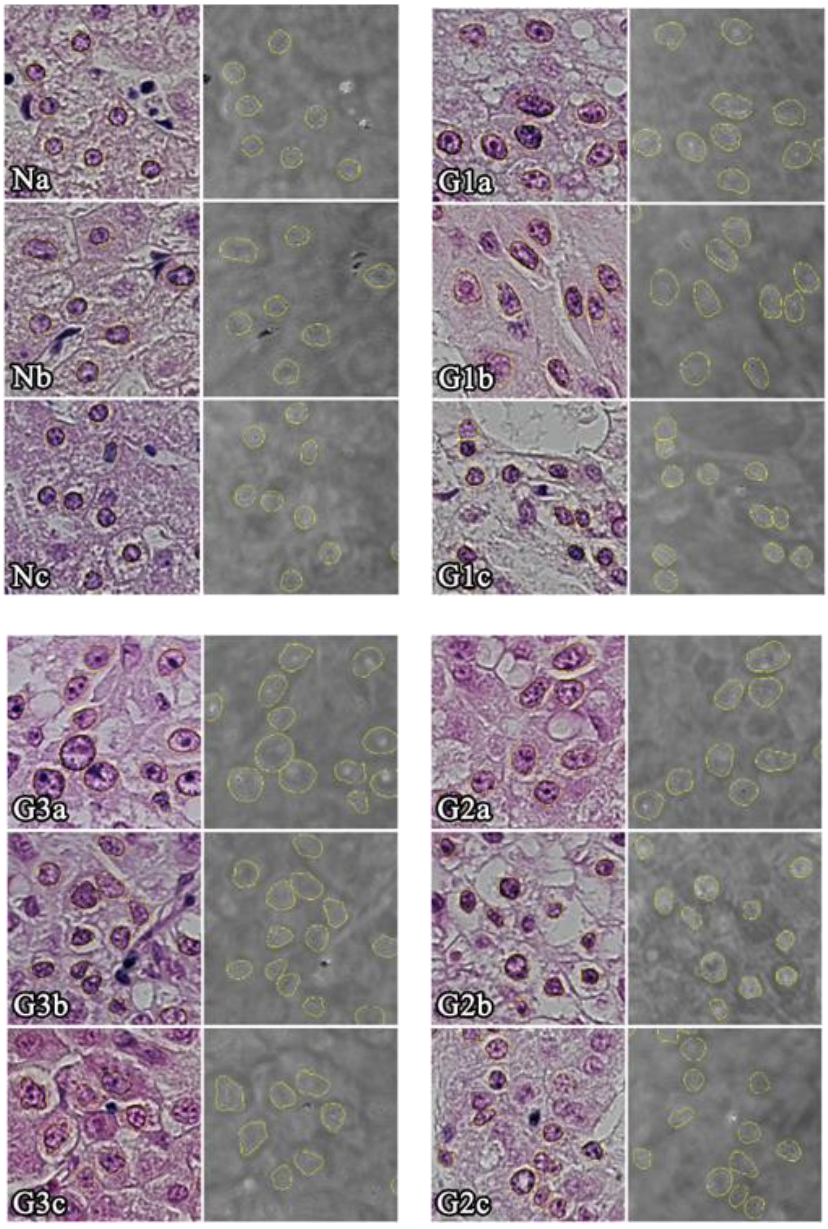

Fig 4.13: Color and phase images

From Table 4.2 below, it can be observed that HCC nuclei have larger area and perimeter than normal nuclei which is a known fact in histopathology.

Sample	Area (μm²)	Perimeter (μm)	Mean phase (rad)	Phase std. dev.
Na	37.5 ± 0.4	39.0 ± 0.2	5.27 ± 0.03	0.42 ± 0.01
Nb	46.4 ± 0.9	44.1 ± 0.4	5.15 ± 0.04	0.39 ± 0.01
Nc	38.0 ± 0.5	39.3 ± 0.3	5.18 ± 0.02	0.40 ± 0.01
G1a	36.0 ± 0.5	38.9 ± 0.3	5.34 ± 0.03	0.31 ± 0.01
G1b	61.4 ± 1.7	53.4 ± 0.7	5.20 ± 0.04	0.35 ± 0.01
G1c	68.1 ± 1.7	54.7 ± 0.7	5.13 ± 0.04	0.36 ± 0.01
G2a	43.7 ± 0.7	42.8 ± 0.3	5.03 ± 0.03	0.30 ± 0.01
G2b	42.6 ± 0.8	42.3 ± 0.4	5.39 ± 0.02	0.43 ± 0.01
G2c	70.2 ± 2.0	55.7 ± 0.8	5.07 ± 0.01	0.37 ± 0.01
G3a	52.8 ± 1.2	48.1 ± 0.6	5.11 ± 0.01	0.35 ± 0.01
G3b	55.6 ± 1.3	48.9 ± 0.6	5.08 ± 0.02	0.33 ± 0.01
G3c	61.2 ± 1.4	52.3 ± 0.6	5.17 ± 0.02	0.40 ± 0.01

Table 4.2: Nuclei morphological and phase features

Figs. 4.14 and 4.15 show the scatter plots of phase mean vs. area and phase mean vs. phase standard deviation.

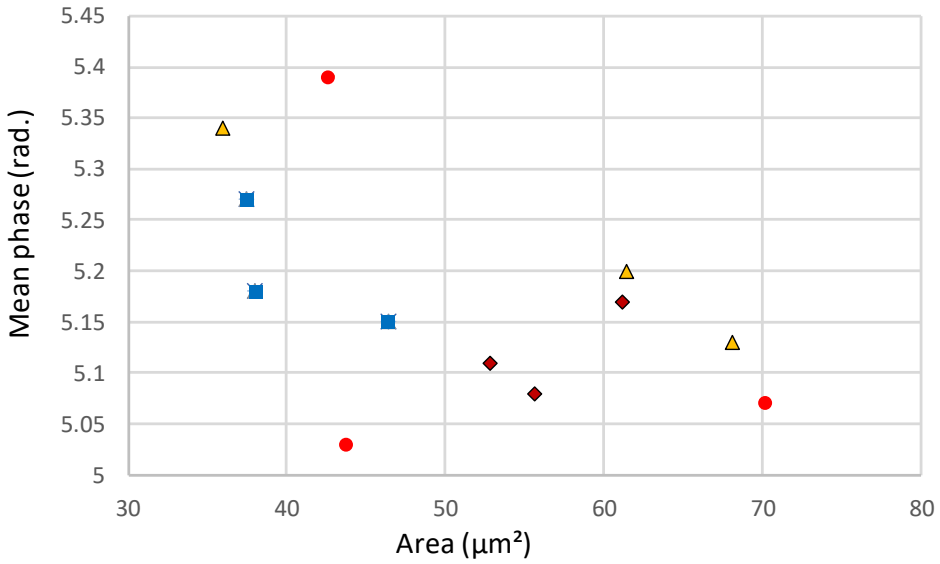

Fig 4.14: Scatter plot of area vs. mean phase, where ■ N, △ G1, ● G2, ◆ G3.

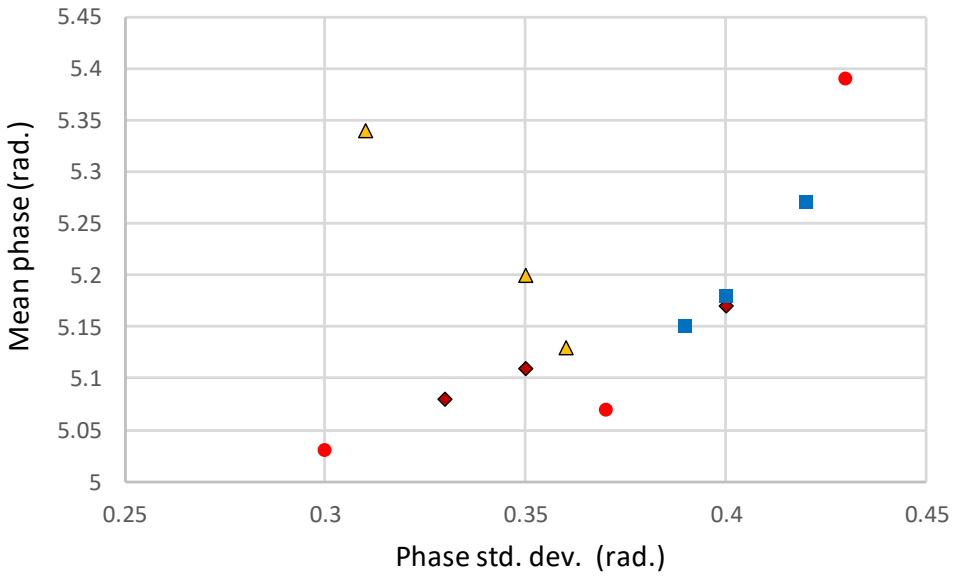

Fig 4.15: Scatter plot of standard deviation and mean of phase, where ■ N, △ G1, ● G2, ◆ G3.

The HCC nuclei are relatively smaller phase modulation and deviation. In Fig. 4.15, the HCC can be characterized as small mean and standard deviation of phase image, except for G2b and G3c. G3c. In those cases, they can be identified using area features. The characteristics of G2b case will be discussed later.

In previous work (Benzerdjeb. N. 2016, Pham. HV. 2016), the phase mean can be used to discriminate cancer and non-cancer cells. In case of cytological samples, the phase mainly represents the thickness of the cell, not the refractive index change. Since the standard deviation of phase expresses the difference between the HCC and normal nuclei, it will be beneficial to focus on texture features e.g. GLCM features, which are shown below.

Sample	ASM (10^{-3})	Contrast	Homogeneity (10^{-3})
Na	1.19	572.5	60.25
Nb	0.97	492.7	61.36
Nc	1.16	588.5	57.22
G1a	1.18	540.8	56.60
G1b	0.70	513.7	57.12
G1c	0.67	536.3	58.00
G2a	0.99	550.9	55.25
G2b	1.03	570.3	59.83
G2c	0.61	573.2	54.23
G3a	0.81	555.5	54.86
G3b	0.83	483.2	62.52
G3c	0.68	548.3	56.06

Table 4.3: Average nuclei GLCM features from bright-field

Sample	ASM (10^{-3})	Contrast	Homogeneity (10^{-3})
Na	3.67	99.19	238.45
Nb	3.34	78.31	234.37
Nc	3.71	93.47	235.80
G1a	4.46	47.73	270.18
G1b	4.25	44.31	300.30
G1c	3.81	52.17	275.88
G2a	4.94	32.57	301.80
G2b	3.22	80.42	237.06
G2c	3.89	55.65	283.12
G3a	3.85	58.78	261.13
G3b	4.13	45.50	288.12
G3c	4.05	67.84	287.70

Table 4.4: Average nuclei GLCM features from phase image

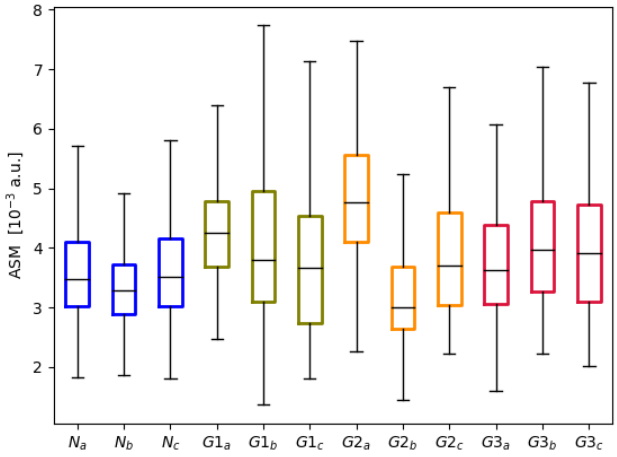

Fig 4.15. GLCM ASM from phase image

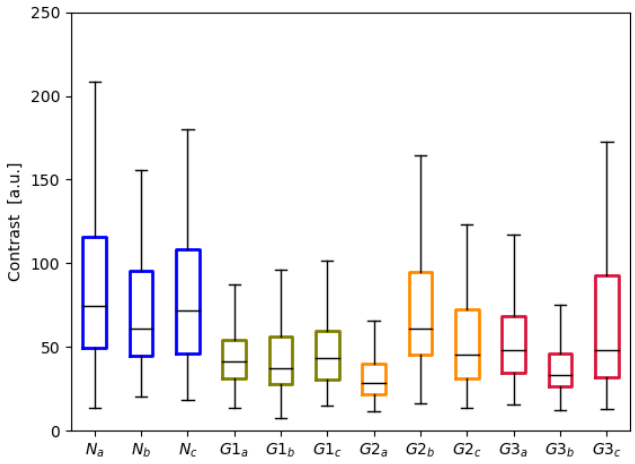

Fig 4.16 GLCM contrast from phase image

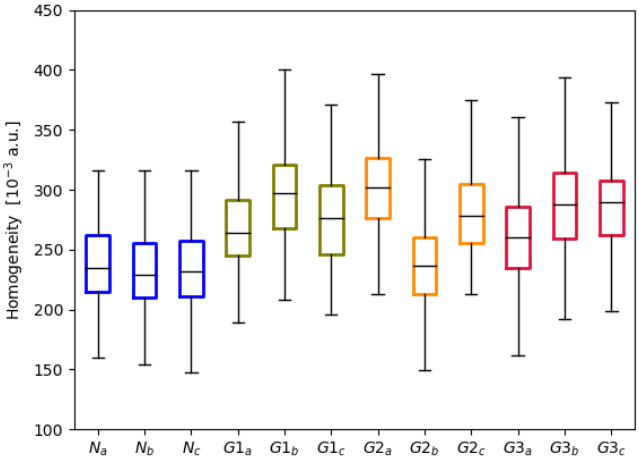

Fig 4.17: GLCM homogeneity from phase image

The distinction between normal and cancer nuclei in phase image can be observed in the GLCM contrast (Fig. 4.16) and homogeneity (Fig. 4.17) features of the phase image. In contrast, the difference is not much apparent in GLCM features in the bright-field images in comparison to the phase images.

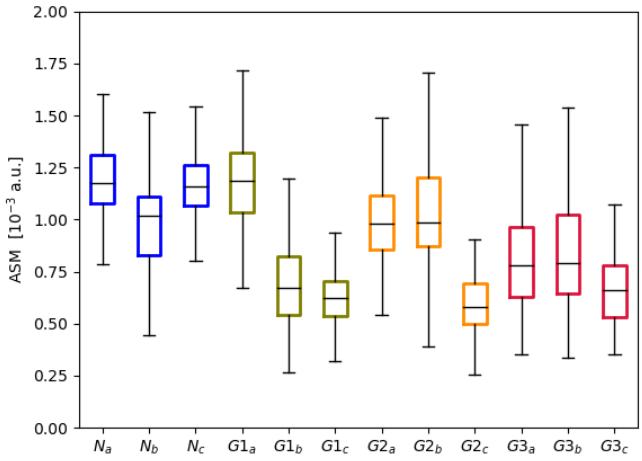

Fig 4.18. GLCM ASM from bright-field image

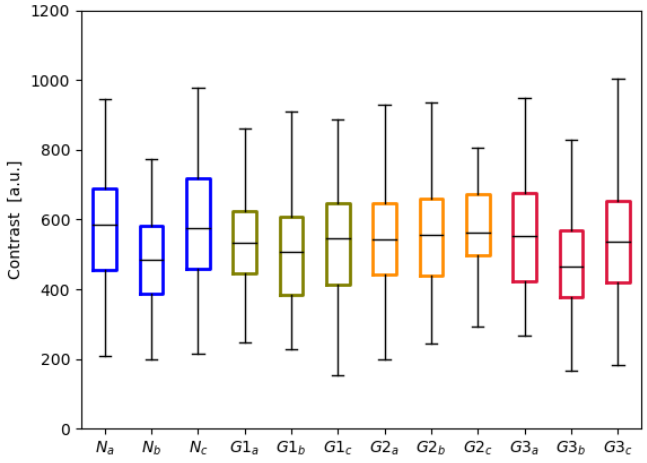

Fig. 4.19: GLCM contrast from bright-field image

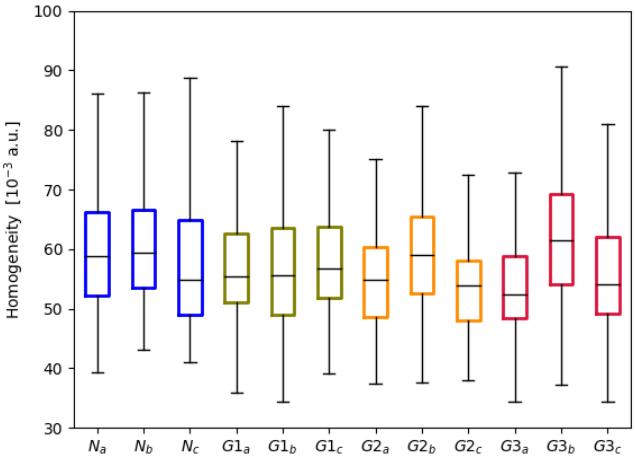

Fig 4.20: GLCM homogeneity from bright-field image

Figs. 4.21 and 4.22 show the scatter plots of GLCM homogeneity, contrast, and ASM texture features calculated from the phase image. In Fig. 4.21, the relationship between the GLCM homogeneity and mean phase is depicted. In both results, the normal and HCC are clearly separated except for the G2b case.

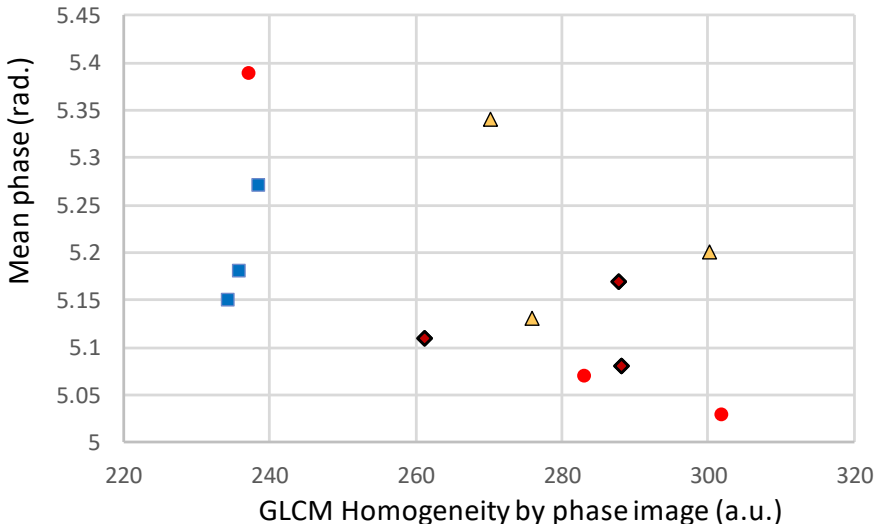

Fig 4.21: GLCM homogeneity by phase vs. mean phase. The same markers as Figs. 4.14~4.15 are used.

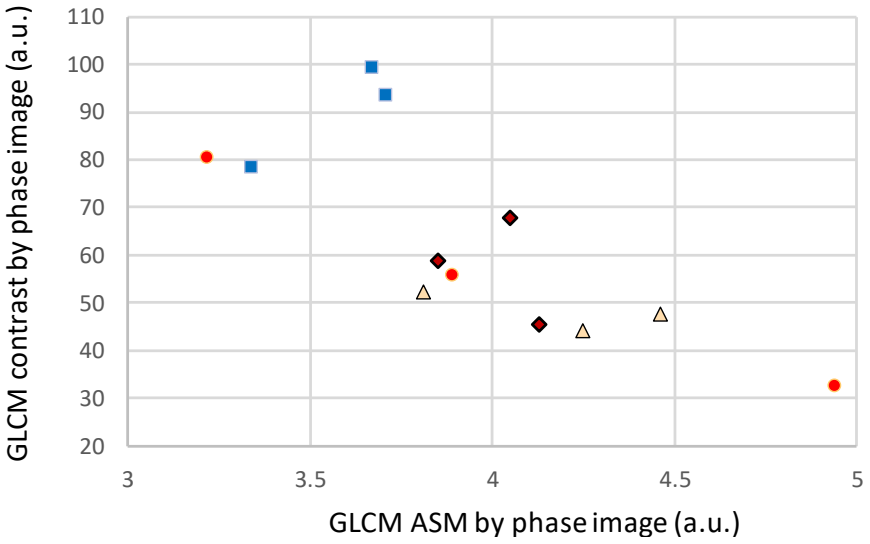

Fig 4.22: GLCM ASM by phase vs. GLCM contrast by phase.

The plot of the std. dev. and GLCM contrast of phase image is shown in Fig. 4.23. Both the std. dev. and contrast are small in most cancer cases, and in the higher std. dev. region, the contrast is relatively smaller in the rest of cancer cases.

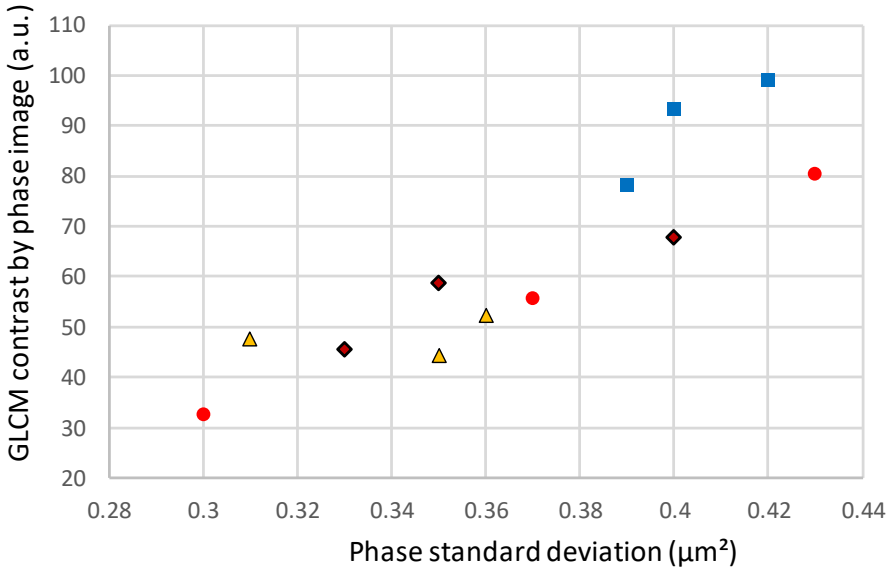

Fig 4.23: Standard deviation of phase vs. GLCM contrast by phase.

Next, a simple nuclei classification system is developed to demonstrate the application of measured phase features. The classifier is based on Support Vector Machine (SVM) with Radial Basis Function as kernel. In the dataset, each HCC grade (N, G1, G2, G3) is consisted of 3 cores and each core has a total of 100 nuclei, totaling 1200 nuclei. The dataset is spitted into 80% training and 20% test data. Each sample core has its own classifier. The optimum parameter of regularizer and gamma constant were determined from grid search in 10-folds cross validation on training data. The classifier will predict which core does a nucleus belongs to and thus giving the predicted grade as well. Four classification models with different combinations of features were investigated. The accuracy is evaluated on how much accurate the model can classify between HCC grades, and binary classification of normal cells vs HCC.

The classification results are summarized as follows.

Model (Features combination)	Grade classification accuracy [%]		
	Correctly classify	Incorrectly to higher grade	Incorrectly to lower grade
Morphological features (area, perimeter,circularity)	58.3	14.2	27.5
Morpho + GLCM Phase + Mean Phase + Std.Dev Phase	70.8	10.4	18.8
Morpho + GLCM Bright Field	66.6	13.3	20.1
All features	65.0	15.4	19.6

Table 4.5: HCC grade classification result using SVM

Model (Features combination)	Confusion matrix of HCC classification [%]				
	True Positive	True Negative	False Positive	False negative	Accuracy (TP+TN)
Morphological features (area, perimeter,circularity)	67.1	15.4	5.0	12.5	82.5
Morpho + GLCM Phase + Mean Phase + Std.Dev Phase	72.9	16.6	3.8	6.7	89.5
Morpho + GLCM Bright Field	72.1	17.9	2.5	7.5	90.0
All features	73.0	16.0	4.6	6.4	89.0

Table 4.6: Normal vs HCC nuclei classification result using SVM

From the results above, homogeneity is larger in cancer cases except for G2b, in comparison with normal cases, as shown in Fig. 4.17. By definition, homogeneity features becomes larger when there are many pixels with adjacent neighbors that have similar value. On the other hand, GLCM contrast behaves oppositely i.e. it gets larger when there are adjacent pixels have large value difference. In normal liver cells, the heterochromatin usually accumulated closely to the nuclear envelope forming an apparent structure. However, in HCC cells, there are cases where it becomes more scattered as smaller structures. Thus, the nuclei texture appears to be more smooth and homogenous when imaged using diffraction limited imaging system.

Regarding the sample G2b, it has the highest mean phase among the dataset. By referring the color bright-field image, the tissue in G2b is consisted of clear cells. It is well known that nuclei in clear cells tend to be smaller and denser. Thus, clear cell cases should be characterized in different manner, for example, their nuclei are smaller and mean phase is higher (refer Table 4.2). Alternatively, the use of features in cytoplasm may be feasible, since the texture becomes mostly vanished in clear cells. In this experiment, clear cells were found only in G2b. In future this issue can be addressed by capturing a larger sample database.

From the classification test, it is apparent that morphological features alone are not sufficient for both HCC grade and binary classification of HCC nuclei. Adding textural features (either phase or intensity) into the classifier will significantly increase accuracy for grading and binary classification. Despite nearly only 70% accuracy, it is sufficient to demonstrate the potential of HCC grading using only morphological and phase texture. In real practice, the classification is conducted on ROI basis instead, thus better understanding should be achieved by analyzing multiple nuclei. In this test, classification accuracy does not increase when combining all features. Possible explanation here is there might be few insignificant features, or there are features that are correlated with each other. This problem can be solved by conducting detailed correlation or variance analysis on these features. Moreover, better accuracy might be possible by further exploring other phase features which is subject for future works.

4.6. Conclusion

In this chapter, the quantitative phase of normal and HCC hepatocytes were measured using DH. Upon analysis, texture features obtained from DH were found to give information different from the color image, which is useful for classifying Hepatocellular Carcinoma and normal cases.

One of the most important advantages of DH in digital pathological image analysis is the possibility of using unstained samples. By developing pathological diagnosis without staining procedure, queue time can be greatly reduce thus gives faster diagnosis. This is mostly beneficial in a region where the pathologist-patient ratio is very low, e.g. in developing countries.

On similar note, it might be helpful during surgery procedure in case the surgeon needs a quick diagnosis on the tissue taken from operated organs. Moreover, the texture analysis is not limited to sliced tissue but also applicable for living cell imaging, in addition to quantitative phase information which DH has been currently utilized. This kind of analysis will provide better information in understanding the cell characteristics, and it will be useful for conventional DH applications including blood cell analysis and tissue engineering for regenerative medicine.

Chapter 5

Digital holography-assisted 3-D bright-field image reconstruction

In this chapter, a brief review on Whole Slide Image (WSI) scanner as current imaging tool in digital pathology. Then, the current issues with 3-D imaging for digital pathology will be explained. Next, a novel 3-D image processing technique that enables color object reconstruction and refocusing by utilizing digital holography will be introduced. Finally, a simulation result and discussion of proposed method will be shown.

5.1. Whole Slide Image (WSI) scanner as imaging tool in digital pathology

As explained in chapter 2, the invention of whole side image (WSI) scanner has greatly enhanced the advancement of digital pathology. Pathological samples can be imaged automatically in a very short time. One of the main advantages of WSI scanner is it can scan the sample in Z-axis at a precise step, making it useful for imaging thick sample. The resulting image set is called z-stack, which is similar to image viewed at different focus plane in conventional microscope. Despite this, most image processing technique in digital pathology mainly revolves around 2-D information. Fortunately, in recent reports, more researchers are now heading towards 3-D sample reconstruction. (Ilaria J. et.al. 2018)

The main reason why 3-D imaging of pathological sample is difficult lies behind the physical limitation of imaging system. Conventional microscope and WSI scanner usually utilize an objective lens with high numerical aperture (NA) to get resolution close to diffraction limit. This however comes at a cost, because the depth of field is inversely related to NA.

$$\text{Depth of field, d} = \frac{\lambda \cdot n}{NA^2} \quad (5.1)$$

Thus, when imaging a thick sample, the object that is slightly away from the front focal plane will appear blurry in the image plane. For this reason, histological samples are usually sliced into a very thin layer (5~20μm) to increase the S/N ratio. It is common for only 1–2 slides are evaluated per tissue block (Kohl SK 2011). In order to capture the whole block, pathologist need to prepare multiple thin slices which is very labor extensive.

In conventional cytopathology, the 3-D structure e.g. how the cells are stacked can give meaningful information during the diagnosis. Still, imaging the z-stack will require capturing multiple images which can be time and memory consuming.

5.2 Color object reconstruction and refocusing using bright-field image and single wavelength digital holography

In this section, a novel image processing technique that combine incoherent (bright-field) and coherent (DH) imaging will be proposed. The proposed method will enable color bright-field image refocusing without the need of capturing z-stack images. The key idea behind this technique is to use reconstructed image from digital holography as a support for deconvolution process on bright-field image. Another main advantage of this method is the resulting image has similar blur properties as incoherent system and it only require digital hologram from a single channel to be captured.

5.2.1 Incoherent and coherent image model

In an incoherent imaging system such as bright-field microscopy, the relationship between input (object) and the resulting output (image) can be modelled as a sum of convolution between light coming from the object and the system point spread function (PSF). This can be expressed as:

$$\mathrm{b}(x,y) = \int i(x,y,z) * p(x,y,z)\, dz \quad (5.2)$$

Here, $i(x, y, z)$ is the intensity of 3D object, $p(x, y, z)$ is the system's 3-D incoherent PSF of the optical system and $*$ is the convolution operator. The PSF can be determined through experimental measurement or estimated using mathematical model such as (Born and Wolf 2003).

For coherent imaging, the complex amplitude at the back focal plane $\mathrm{v}(x, y)$ can be expressed as sum of diffracted light coming from multiple z-planes.

$$\mathrm{v}(x, y) = \int u(x, y, z) * h(x, y, z)\, dz \quad (5.3)$$

Here $u(x, y, z)$ is the complex amplitude of the 3D object and $h(x, y, z)$ is the wave propagation kernel. Alternatively, by using angular spectrum method and applying convolution theorem, this equation can be expressed as:

$$\mathrm{v}(x, y) = \int \mathcal{F}^{-1}\left\{\mathcal{F}\left(u(x, y, z) \cdot H\left(f_x, f_y, z\right)\right)\right\} dz \quad (5.4)$$

Where

$$H\left(f_x, f_y, z\right) = \begin{cases} \exp\left(j2\pi \frac{z}{\lambda}\sqrt{1 - (\lambda f_x)^2 - \left(\lambda f_y\right)^2}\right) : \sqrt{f_x^2 + f_y^2} < \frac{1}{\lambda} \\ 0 : others \end{cases} \quad (5.5)$$

$\mathcal{F}$ denotes the 2-D Fourier transform operator in XY direction. The relationship between u and i can be expressed as:

$$|u(x, y, z)|^2 = i(x, y, z) \quad (5.6)$$

5.2.2 Image refocusing in incoherent and coherent system

Image refocusing in incoherent system can be viewed as deconvolution of $b(x, y)$ via inverse filtering. The process can be relatively straightforward if multiple $b(x, y)$ i.e. the z-stack are captured. If not, the deconvolution process is difficult because first, there are more unknown than known values. Second, the Fourier coefficient of the

PSF can be close to zero thus most of the information is now lost and would not be easily recovered from just using an inverse filter.

For coherent system, the image can be refocused by calculating the wave propagation of $v(x, y)$. However, since $v(x, y)$ consists of light wave coming from multiple planes, the out-of-focus object in the refocused image will appear as diffraction pattern thus reducing the S/N ratio.

Determining the complex amplitude volume $u(x, y, z)$ from $v(x, y)$ is an ill-posed problem. Fortunately, by using compressive sensing approach a satisfactory reconstruction is possible (David J. Brady et.al 2009).In their proposed a method, two objects separated in z-axis were reconstructed from a single Gabor hologram by solving an optimization problem:

$$\hat{\eta} = \arg\min_{\eta} \frac{1}{2}\|g - Q\eta\|^2 + \gamma\phi(\eta) \quad (5.7)$$

Here, η is the 3D object scattering density, g is the captured Gabor hologram and Q is the wave propagation matrix that generates Gabor hologram. They used 2-D total variation as the regularization function ϕ and γ is the regularization weight. The optimization was solved using two-step shrinkage/thresholding algorithm (TwIST).

5.2.3 Principle of two-step shrinkage/thresholding algorithm (TwIST)

In a linear system, the relationship between input and output can me modelled in a matrix form.

$$y = Kx \quad (5.8)$$

Where x is the input, y is the output and matrix K gives the linear mapping of x to y. Suppose we wish to recover x from y, one might be interested in calculating the direct inverse matrix K^{-1}, or use the least-square algorithm. However, these approaches are not feasible when the system is under-determined.

One clever approach to solve this problem is by using the compressive sensing technique. In this method, the value x is assumed to be sparse in certain domain. If we define $\phi(x)$ as a function that map x to that particular domain, we can redefine the inverse problem into an optimization problem.

$$\hat{x} = \arg\min_{x} \frac{1}{2}\|y - Kx\|^2 + \gamma\phi(x) \quad (5.9)$$

Again, solving this is not straight-forward because despite the first term is convex, $\phi(x)$ can be non-differentiable and non-convex. This problem is well researched and there are several algorithms already being proposed. One of them is called Iterative Shrinkage/Thresholding (IST). The algorithm is defined as:

$$\hat{x}_{t+1} = (1-\beta)\hat{x}_t + \beta\Psi_\gamma\left(\hat{x}_t + K^T(y - K\hat{x}_t)\right) \quad (5.10)$$

Here, β and γ are constants and $\Psi_\gamma(\dot{x})$ is called de-noising function, which is obtained by solving a simpler problem:

$$\Psi_\gamma(\dot{x}) = \arg\min_{x} \frac{1}{2}|\dot{x} - x|^2 + \gamma\phi(x) \quad (5.11)$$

A modified version that claims to have faster convergence is called two-step shrinkage/thresholding algorithm (TwIST) (Jose. M. and Mario AT 2007). Here, $\hat{x}$ is computed iteratively using the following scheme (5.12):

$$\hat{x}_1 = \Gamma_\lambda(\hat{x}_0)$$

$$\hat{x}_{t+1} = (1-\alpha)\hat{x}_{t-1} + (\alpha - \beta)\hat{x}_t + \beta\Gamma_\gamma(\hat{x}_t)$$

$$\Gamma_\gamma(x) = \Psi_\gamma\left(x + K^T(y - Kx)\right)$$

α, β and γ are constants.

5.2.4. Proposed method

In this section, the proposed method for color image refocusing using single wavelength digital holography will be explained. This method requires the acquisition of two information: color image and digital hologram of a same 3-D object.

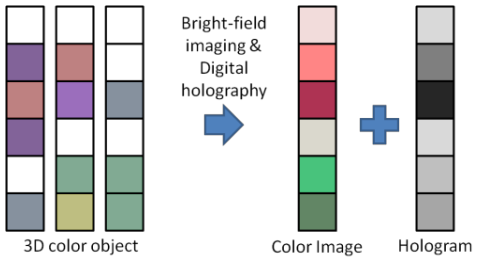

Fig 5.1: Acquisition of color image and digital holography

First, the imaging model for digital hologram is defined as follows. The 3-D object is illuminated by a plane wave. The light wave is modulated by modulation function η and captured as digital hologram. The conjugate plane of the hologram plane with respect to the objective lens is defined as 'plane C'.

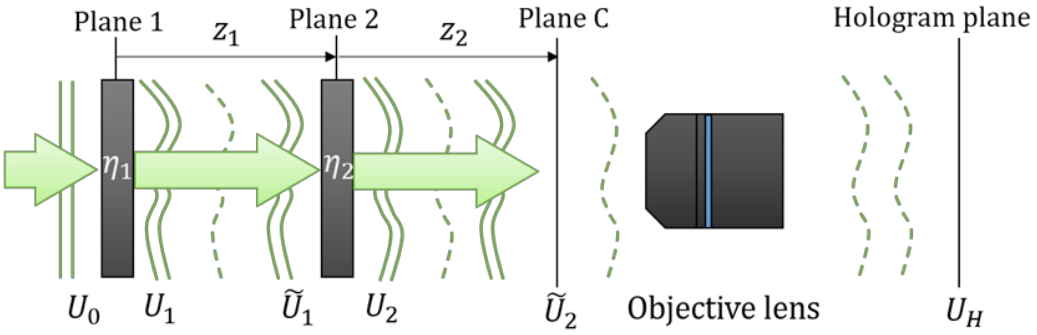

Fig 5.2: Imaging model for digital holography.

Now consider there are two object planes with complex modulation of $\eta_1(x,y)$ and $\eta_2(x,y)$ which is separated by a distance $\eta_2(x,y)$, located at plane 1 and 2 as shown in figure above. From this, $\eta_m(x,y) = 1 - t_m(x,y)$ where $t_m(x,y)$ represents the complex amplitude transmittance of the object at plane-*m*. Thus $|\eta_m\ (x,y)|$ is 0 in case the light is

fully transmitted otherwise equals to 1 when the light is entirely lost due to scattering or absorption.

When plane 1 is illuminated with a plane wave $U_0\ (x, y)$, the transmitted light wave can be written as:

$$U_1\ (x, y) = U_0\ (x, y) - U_0\ (x, y)\ \eta_1\ (x, y) = U_0\ (x, y)[1 - \eta_1\ (x, y)] \quad (5.13)$$

It propagates until it reaches plane 2.

$$\widetilde{U}_1\ (x, y) = F_R\ \{U_1\ (x, y), z_1\} \quad (5.13)$$

Here, $F_R\ \{\cdot, z\}$ is the wave propagation operator, e.g. convolution of the Fresnel or angular spectrum kernel at propagation distance of z.

Moving on to the wave that comes out of plane 2,

$$U_2\ (x, y) = \widetilde{U}_1\ (x, y)[\ 1 - \eta_2\ (x, y)] \quad (5.14)$$

Consequently, the wave at plane C is given by

$$\widetilde{U}_2\ (x, y) = F_R\ \{U_0\ (x, y), z_1 + z_2\ \} - F_R\ \{U_0\ (x, y)\eta_1\ (x, y), z_1 + z_2\ \}]$$

$$-F_R\ \{\eta_2\ (x, y)F_R\ \{U_0\ (x, y), z_1\ \}, z_2\ \}$$

$$+F_R\ \{\eta_2\ (x, y)F_R\ \{U_0\ (x, y)\eta_1\ (x, y), z_1\ \}, z_2\ \} \quad (5.15)$$

This results 4 terms on the right-hand side.

1) Illumination plane wave.
2) Modulated waves from object 1.
3) Modulated wave from object 2.
4) Wave modulated by both object 1 and object 2.

Here, equation 5.15 can be approximated into simpler form using these assumptions:

1) If the object is sparse, there is less chance for the light waves to be modulated multiple times. Thus, the fourth term will be much smaller relative to other terms and can be omitted.
2) If the magnitude of η_1 and η_2 are small, i.e.the objects are semitransparent then fourth term will be near to zero.

By following these assumptions, the approximation can be written as follow.

$$\widetilde{U}_2\,(x,y) \cong U_0\,(x,y)\;\; exp\,\{jk(z_1+z_2\,)\} - F_R\,\{U_0\,(x,y)\eta_1\,(x,y), z_1+z_2\,\}$$

$$-F_R\,\{U_0\,(x,y)\eta_2\,(x,y) ex\,p(jkz_1\,)\,, z_2\,\} \quad (5.16)$$

k is the wave number of the illumination light. Objective lens is then used to magnify $\widetilde{U}_2\,(x,y)$ into $U_H\,(x,y)$.

Further generalizing the model which has of N_z planes;

$$\widetilde{U}_H(x,y) \cong U_0(x,y)\exp(jkd_1) - \sum_{m=1}^{N_z} \mathcal{F}_{\mathrm{R}}\{U_0(x,y)\eta_m(x,y)\exp[jk(d_1-d_m)]\,, d_m\}\,.$$

(5.17)

d_m is the distance between m-th plane to the object plane.

Using similar approach, the imaging system model for incoherent imaging can be expressed as follows:

$$\tilde{J}(x,y) \cong J_0(x,y) - \sum_{m=1}^{N_z} [J_0(x,y)\mu_m(x,y)] * p_m(x,y)$$

(5.18)

Here, the intensity modulation function and the point spread function at the m-th plane are defined as $\mu_m\,(x,y)$ and $p_m\,(x,y)$. The resulting BF image is $\tilde{J}(x,y)$, $J_0\,(x,y)$ is the illumination intensity and $*$ represents the convolution operator.

Figure 5.3 below depicted the general outline of proposed method. The reconstruction process is divided into two stages. Firstly, the 3-D object modulation $\eta_m\ (x, y)$ is reconstructed from DH via compressive holography.

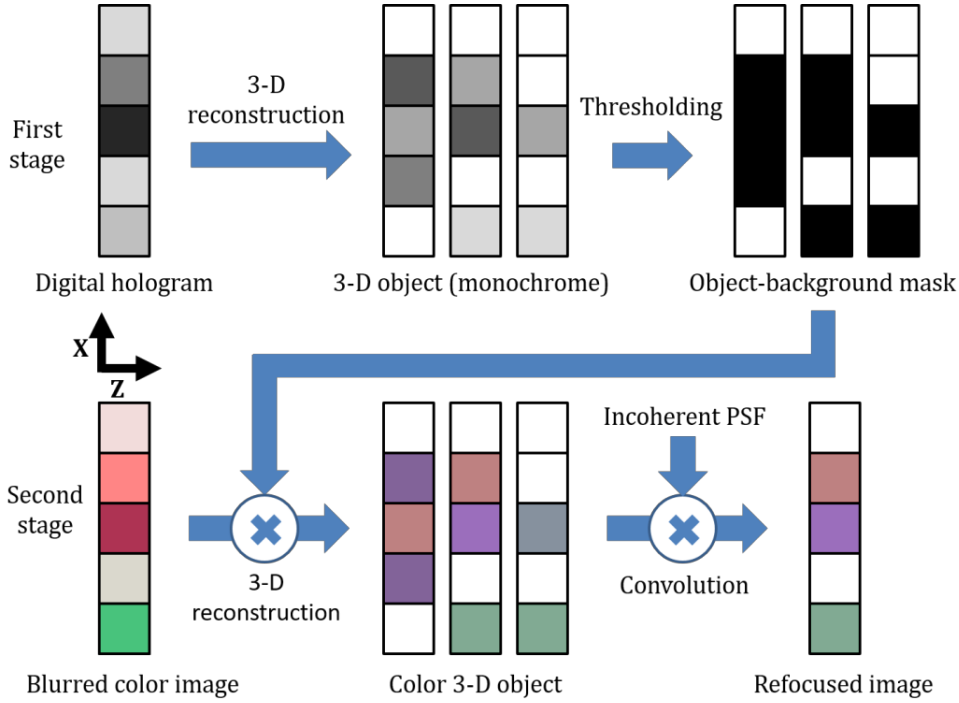

Fig 5.3: Outline of proposed algorithm

This is done by we solving equation below using monotonic TwIST:

$$\hat{\boldsymbol{\eta}} = \arg\min_{\boldsymbol{\eta}} \frac{1}{2}\|\boldsymbol{u} - \boldsymbol{W\eta}\|^2 + \xi_1 \phi(\boldsymbol{\eta}) \quad (5.19)$$

where $\boldsymbol{\eta}$ is the object's 3-D complex modulation function in the form of $(N_x \times N_y \times N_z) \times 1$ sized matrix. Here, $u = u_0\, exp(jkd_1) - \tilde{u}_H$. Its matrix form $\boldsymbol{u}$ has a size of $(N_x \times N_y) \times 1$. $\boldsymbol{W}$ is the forward wave propagation matrix with a size of $(N_x \times N_y) \times (N_x \times N_y \times N_z)$.

The multiplication of $\boldsymbol{W\eta}$ is can be optimized using fast Fourier transform based convolution. 2-D total variation is used as the regularization function ϕ, and ξ_1 is the regularization weight.

Afterwards, a binary mask that distinguish the object and background is generated by applying a thresholding process such as Otsu's method on $|\hat{\eta}|$. The resulting mask $\boldsymbol{M}$ has elements equals to 1 if it corresponds to object else 0 if it's a empty voxel.

In the second stage, the binary mask is utilized to assist the reconstruction of $\mu_m\ (x, y)$ from the BF image. The key concept is to assume a correlation between channels and there is no voxel with pure R, G, and B color. The color object can be reconstructed as by solving the next equation using TwIST:

$$\hat{\boldsymbol{\mu}} = \arg\min_{\boldsymbol{\mu}} \frac{1}{2}\|\boldsymbol{J} - \boldsymbol{P}\boldsymbol{\mu}\|^2 + \xi_2\phi(\boldsymbol{\mu}) \quad (5.20)$$

Here, $\boldsymbol{\mu}$ is the matrix form of the 3-D intensity modulation function. $\boldsymbol{J} = \boldsymbol{J}_0 - \tilde{\boldsymbol{J}}$. $\boldsymbol{P}$ is the forward convolution matrix. ϕ is the 2-D total variation regularization function and ξ_2 is the regularization weight.

The denoising step in TwIST is modified to incorporate the masking process i.e. the de-noised $\hat{\boldsymbol{\mu}}$ is multiplied by mask $\boldsymbol{M}$ element-wise. The reconstruction is done on all RGB channels using same mask $\boldsymbol{M}$. Once $\hat{\boldsymbol{\mu}}$ is reconstructed, the color image can be generated using eq. 5.18. Finally, image refocusing can be done by shifting the index m during the convolution calculation.

5.2.5. Simulation result and discussion

For simulation, 4 objects (Alphabet-Number pairs) were placed at different z-planes as shown in figure below.

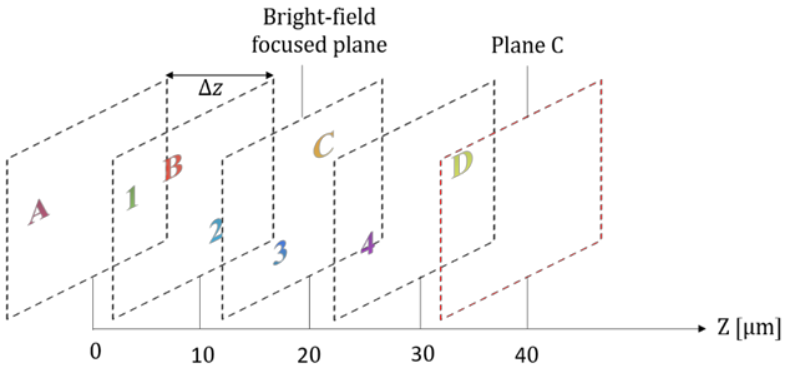

Fig 5.4: Simulation model.

Each object has dominant color e.g. red, green, blue and gray respectively. The objects were designed with a slight gradient texture to make sure no pure RGB pixels exist. The background of each plane was set to be fully transparent. The light wave at the image plane was calculated using the forward model as described in previous section. The origin of z-axis was set to be plane A1.

Simulation parameters are summarized in table below.

Parameter	Value
Plane resolution	512×512 pixels
Wavelength illumination laser in DH	λ = 532 nm
Object plane sampling size	0.1675 μm
Object layer count	4
Distance between planes (Δz)	10 μm
Offset to Plane C	10 μm

Table 5.1: Simulation parameters

In BF mode, the object was illuminated with white light. The simulated PSF for BF was generated by fitting a Gaussian function to PSF measured from an objective lens with NA 0.75. The highest focus was set on the object at the third plane (C3) i.e. by setting the object closer to objective lens during BF acquisition.

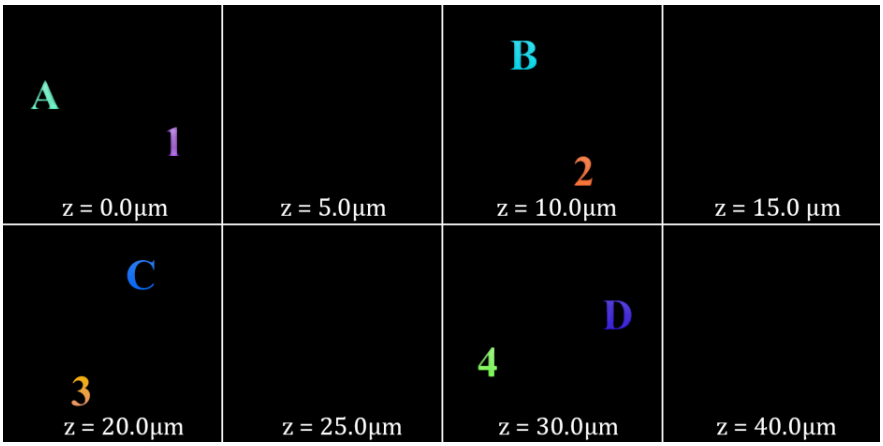

Fig. 5.5: Ground truth of intensity modulation function, µ.

Figure 5.5 depicted the object intensity modulation function used in the simulation. For complex modulation, the values were generated from intensity modulation function using the relationship below.

$$|\eta_m(x,y)|^2 = \mu_m(x,y) \quad (5.21)$$

The phase of η_m was set to be random $N(\pi, 0.5)$ [rad] to mimic phase texture of real object. Figure 5. 6 shows the amplitude of light wave at plane C and the color BF image. Only these two images were used as inputs during the reconstruction process.

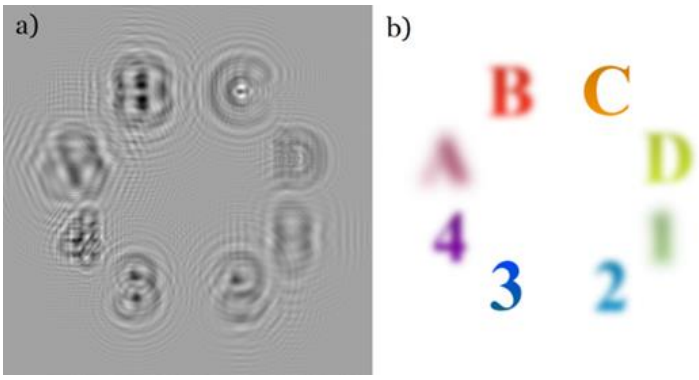

Fig. 5.6: Amplitude of object wave and (b) color BF image. Object A1 appears the most blurred in (b) as it is farthest from plane C.

The 3-D reconstruction results are depicted in Figure 5.7-5.8. Other than few artifacts in the intermediate planes, the complex modulation was successfully reconstructed using the compressive holography, as shown in Figure 5.7. These errors were removed during the thresholding process

Figure 5.8 shows the reconstruction result of intensity modulation. It can be seen that the objects were properly reconstructed to its proper plane. Furthermore, the intermediate planes are completely empty due to the binary mask. Yet, few errors appear at the object's edges because of the imperfect mask shape. Final root-mean-square error (RMSE) of $\hat{\mu}$ was calculated to be 4.50×10−3.

For comparison, Figure 5.9 shows the reconstruction using only color BF image. Here, regardless sparsity prior regularization was imposed, TwIST failed to correctly reconstruct the 3-D object. This is indeed expected as the Gaussian PSFs have high similarity. In other words, the matrix does not abide restricted isometric property which is crucial for solving the under-determined system.

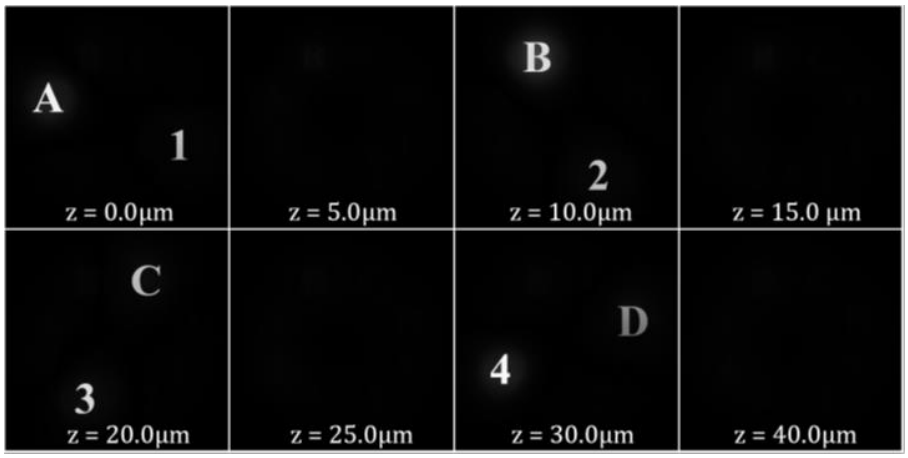

Fig. 5.7: Reconstructed amplitude of complex modulation function $\hat{\eta}$

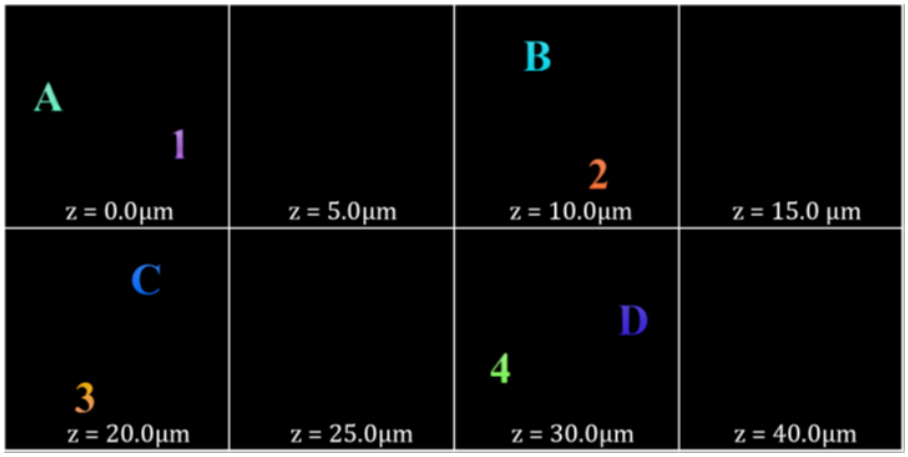

Fig. 5.8: Reconstructed intensity modulation function $\hat{\mu}$

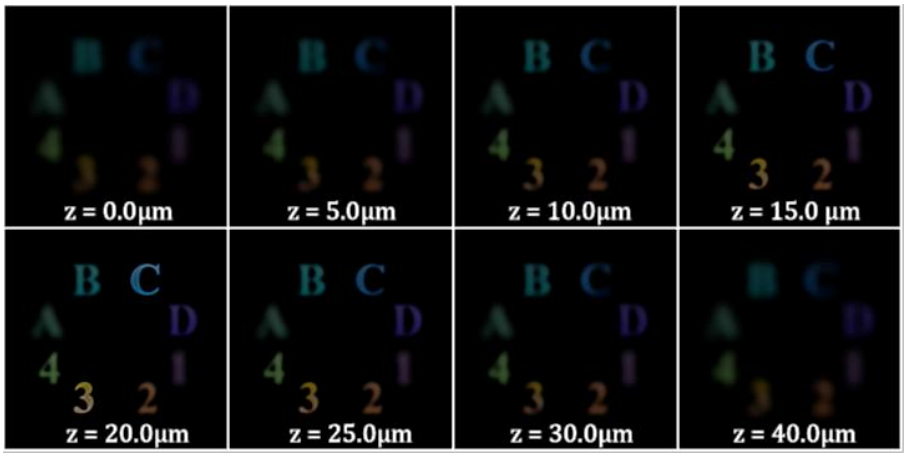

Fig. 5.9. Same as Fig. 5.8. but without DH assistance. (Contrast enhanced for clarity)

In the next simulation, the reconstruction of simulated cell phantom (Figure 5.10) generated from segmented cell nuclei of pathological images were demonstrated. Similar to the previous setup, the cells were distributed into four different planes with slight overlapping between each other in z-axis. Outside of the phantom, all other simulation parameters are exactly same.

The cell reconstruction is shown in Figure 5.11-5.12. The morphological shape of the cell cluster was successfully reconstructed. However, it is important to note here that texture inside the cells becomes blurry. This can be explained by the fact most of the spectral information in the out-of-focus plane is attenuated by the optical system's modulation transfer function. As a result, the final the RMSE was 1.21×10^{-2}, which is larger than the previous simulation.

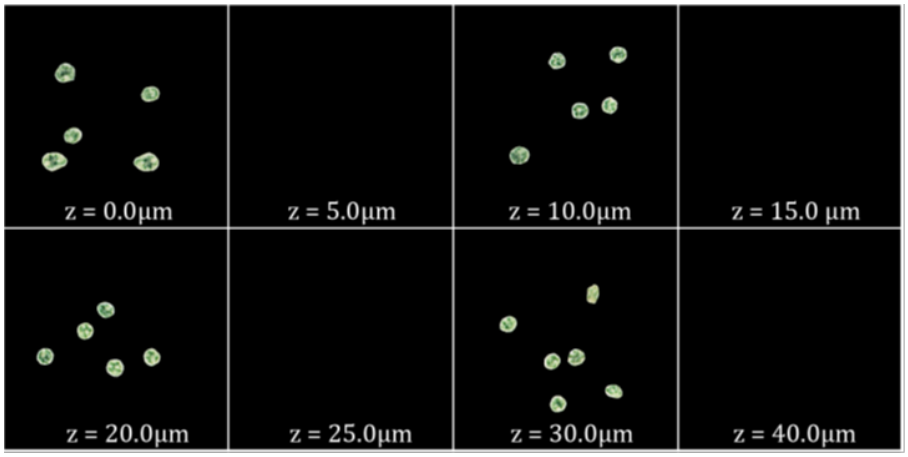

Fig. 5.10: Ground truth μ

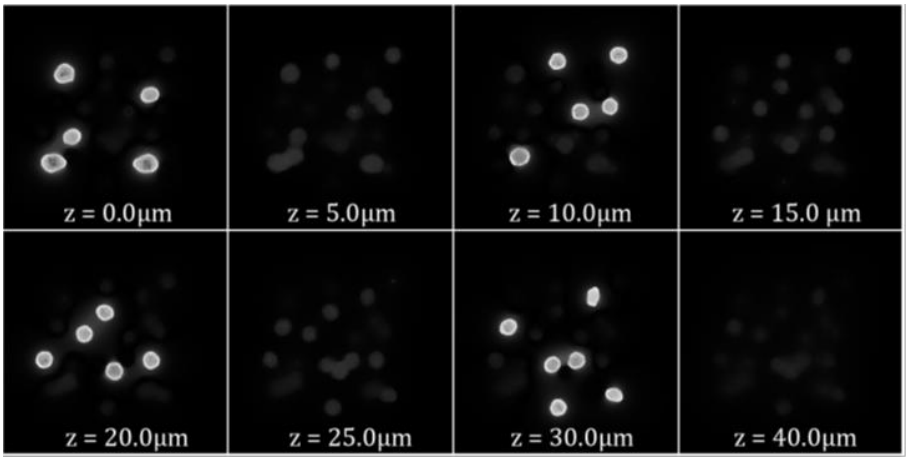

Fig. 5.11: Reconstructed $\hat{\eta}$

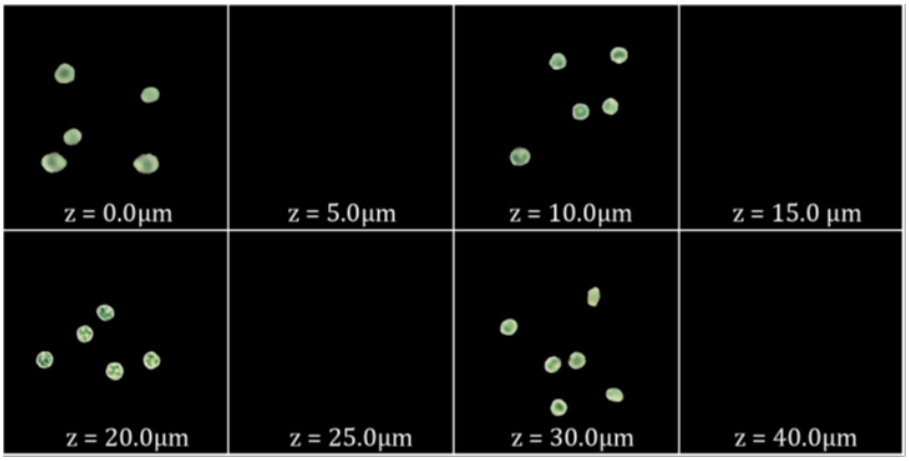

Fig. 5.12: Reconstructed $\hat{\mu}$

5.2.5. Conclusion

In this chapter, a new image processing technique that combine digital holography and bright-field imaging was proposed. The proposed method utilizes digital holography to assist color 3D object reconstruction from bright-field image. The main merit of the proposed method is that it only requires a color BF image and monochrome DH. Furthermore, digital refocusing can be applied to the reconstructed object, while creating natural blur similar to a common optical system due to usage of incoherent PSF. Hopefully, this technique can be applied in digital pathology for capturing and reconstructing the 3D morphological features of cytological samples, without the need of Z-stack images.

Chapter 6

Conclusion

In this study, a hybrid color and quantitative phase imaging system was developed by combining bright-field and digital holographic microscopy. Using the hybrid system, the phase and color image of pathological samples were successfully captured.

In chapter 3, the imaging system was utilized to image cytological samples. The phase images of normal and malignant lymphocytes were analyzed. Based on the experimental investigation, it is found that the spatially-averaged mean value of malignant lymphocytes has bigger dispersion relative to normal cells. This feature might be useful for malignant lymphoma identification purpose. Moreover, the large dispersion might give some insight on the refractive index distribution inside the malignant cell. Future analysis can include samples that has relatively close size. Although the color image was not utilized in the statistical calculation, it is beneficial as reference during the analysis.

In chapter 4, a more detailed study was conducted on texture features inside phase and color images. For this time, a histopathological sample (liver tissue) was used as object of study. From the analysis, it was found that texture features obtained from phase image were different from the color image. These features can be utilized together with other morphological features for classifying and detecting Hepatocellular Carcinoma cases.

In chapter 5, a novel image processing technique that combine incoherent and coherent imaging was proposed. In the proposed method, digital hologram was used to assist color image deconvolution. A simulation was conducted to demonstrate the proposed algorithm. As for application, this technique can be used to refocus bright-field image without the need of z-stack imaging. Nevertheless, the real demonstration via experiment need to be conducted in near future.

List of related publications

(a) Journal papers (Referred)

SH Norazman, T Nakamura, F Kimura, M Yamaguchi, Analysis of Quantitative Phase Obtained by Digital Holography on H&E Stained Pathological Sample, Artificial Life and Robotics, 24, 38–43 (2019). DOI: 10.1007/s10015-018-0468-4

SH Norazman, T Nakamura, M Yamaguchi, Digital holography-assisted 3-D bright-field image reconstruction and refocusing , Optical Review (2020). DOI: 10.1007/s10043-020-00615-7

(b) International conferences

S Hakim, M Yamaguchi and F Kimura, Application of digital holography on diagnosis of malignant lymphoma, 14th Workshop on Information Optics (WIO), Kyoto Japan, (2015). DOI: 10.1109/WIO.2015.7206908

(c) Journal papers (Non-referred)

(d) Domestic conferences

SH Norazman, M Yamaguchi and F Kimura, Phase image analysis of liver tissue with Hepatocellular Carcinoma (HCC), OPJ 2015 (Optics & Photonics Japan) Tokyo Japan, 2015

SH Norazman, M Yamaguchi and F Kimura, Digital Holography & Hepatocellular Carcinoma (HCC): Textural features on phase image, OPJ 2016 (Optics & Photonics Japan) Tokyo Japan, 2016

SH Norazman, T Nakamura, F Kimura et.al. Analysis of Quantitative Phase Obtained by Digital Holography on H&E Stained Pathological Sample, 5th Symposium of the 'Color' of Digital Imaging in Biomedicine, Chiba Japan, 2018

Bibliography

[1] V. Ojansivu et al., “Automated classification of breast cancer morphology in histopathological images,” Diagnostic Pathology, vol. 8, no. Suppl 1. p. S29, 2013.

[2] A. Saito, E. Cosatto, T. Kiyuna, and M. Sakamoto, “Dawn of the digital diagnosis assisting system, can it open a new age for pathology?,” Proc.SPIE, vol. 8676, pp. 8676-8676–16, 2013

[3] Pantanowitz L, Digital Images and the Future of Digital Pathology. Journal of Pathology Informatics 1:15, 2010

[4] Kiyuna T, Saito A, Kerr E et al, Characterization of chromatin texture by contour complexity for cancer cell classification. 8th IEEE International Conference on BioInformatics and BioEngineering, Athens, Greece, Oct 8-10, 2008

[5] Kiyuna T, Saito A, Marugame A, et al, Automatic classification of hepatocellular carcinoma images based on nuclear and structural features. Proc. SPIE 8676, Medical Imaging 2013: Digital Pathology, 86760Y, 2013

[6] Benzerdjeb N, Garbar C, Camparo P et al (2016), Digital holographic microscopy as screening tool for cervical cancer preliminary study. Cancer Cytopathology, 124:573–580

[7] Takeda M, Ina H, Kobayashi S (1982), Fourier-transform method of fringe-pattern analysis for computer-based topography and interferometry. Journal of the Optical Society of America, 72:156-160

[8] Herráez MA, Burton DR, Lalor MJ et al (2002), Fast two-dimensional phase-unwrapping algorithm based on sorting by reliability following a noncontinuous path. Applied Optics, 41:7437-7444

[9] Wienert S, Heim D, Saeger K et al (2012), Detection and segmentation of cell nuclei in virtual microscopy images: A minimum-model approach. Scientific Reports, 2:503

[10] Haralick RM, Shanmugam K, Dinstein I (1973), Textural features for image classification. IEEE Transactions on systems, man and cybernetics, 3:6

[11] R.K. Gupta, S. Naran, S. Lallu, and R. Fauck, "Diagnostic Value of Needle Aspiration Cytology in the Assessment of Palpable Axillary Lymph Nodes," Acta Cytologica, vol. 47, no. 4, 2003.

[12] S. Al-Janabi, A. Huisman, and P. J. Van Diest, "Digital pathology: current status and future perspectives," Histopathology, vol. 61, no. 1, pp. 1-9, 2012.

[13] R. C. Gonzalez and R. E. Woods, "Image segmentation," in Digital Image Processing, 3rd ed. Upper Saddle River, NJ: Prentice-Hall, 2008, pp. 769-778.

[14] R. K. Bista et. al., “Quantification of nanoscale nuclear refractive index changes during the cell cycle”, Journal of Biomedical Optics, Vol. 16(7), 2011

[15] Kohl SK, Lewis SE, Tunnicliffe J, et al. The College of American Pathologists and National Society for Histotechnology workload study. Arch Pathol Lab Med. 2011;135:728–736

[16] David J. Brady et.al, Optics Express Vol.17 Issue 15

[17] P. Wang et. al., “An insight into statistical refractive index properties of cell internal structure via low-coherence statistical amplitude microscopy”, Optics Express, Vol. 18(21), 2010

[18] A New TwIST: Two-Step Iterative Shrinkage/Thresholding Algorithms for Image Restoration,José M. Bioucas-Dias and Mário A. T. Figueiredo, IEEE TRANSACTIONS ON IMAGE PROCESSING, VOL. 16, NO. 12, DECEMBER 2007

[19] Hoa V. Pham et. al., Cancer cytopathology Vol. 124(9), 2016

[20] Xiaoxu Lu et.al,"3D profile reconstruction of biological sample by in-line image-plane phase shifting digital microscopic holography", Optics and Lasers in Engineering 50 (2012) 1431–1435

[21] N. Pavillon et.al. ,"Early Cell Death Detection with Digital Holographic Microscopy", PLoS One, Jan 2012, Vol. 7-1

[22] X. Mo, B. Kemper, P. Langehanenberg, A. Vollmer, J. Xie, and G. v. Bally, "Application of color digital holographic microscopy for analysis of stained tissue sections," Proc. SPIE, vol. 7367, p.736718,2009.

[23] H. Byeon et. al, "Hybrid bright-field and hologram imaging of cell dynamics", Scientific Reports volume 6, Article number: 33750 (2016)

[24] Jansen I et.al, "Histopathology: ditch the slides, because digital and 3D are on show.",World J Urol. 2018 Apr;36(4):549-555

[25] Oliver et.al, "Digital refocusing with incoherent holography", 2014 IEEE International Conference on Computational Photography (ICCP)

[26] F. N. Ghadially. (1997). Ultrastructural pathology of the cell and Matrix. Butterworth-Heinemann

[27] F.Kimura et.al, “Detection of Ki67 expression by analyzing texture of hematoxylin-and-eosin-stained images, the effectiveness of signal intensity, and co-occurrence matrix features”, Anal. Quant. Cyto. 40. 9-19 (2018)

[28] Cherkezyan et al., “Nanoscale changes in chromatin organization represent the initial steps of tumorigenesis: a transmission electron microscopy study”, BMC Cancer 2014, 14:189

Acknowledgement

بسم الله الرحمن الرحيم

Firstly, I would like to express my sincere gratitude to my research supervisor, Prof. Masahiro Yamaguchi for his enormous guidance and support throughout my journey in completing this thesis. Under his supervision, I was blessed to conduct researches, meet wonderful lab mates and dedicated researchers in holography and pathological field. Those were experience that I will never gain in my home country. His support is not limited to research but also on personal life level. I'm also thankful that he offered me position as RA position for multiple projects.

Secondly, I would like to thank Ass. Prof. Tomoya Nakamura for his support and research ideas. His guidance and discussion on topics related to compressive sensing and inverse problem has helped me a lot especially in Chapter 5 of this thesis. Also, I am very grateful to work as RA under his research project.

My sincere thanks also go to Dr. Fumikazu Kimura for his guidance on pathological know-how. He has provided various cytological and histological samples to be used for my research.

I thank my fellow lab mates, specially Holo group members for the insightful discussions and enjoyable moments we had. Finally, I would like to thank UMP for providing 3 years scholarship for my Ph. D program.